UNITED STATES DEPARTMENT OF THE INTERIOR
GEOLOGICAL SURVEY

One and Two-Dimensional Inversion of Magnetotelluric Data across the Basin-Range - Colorado Plateau, Virgin Mountains Area, NW Arizona and SW Nevada.

by

Jeffrey A. Meredith* and Frank C. Frischknecht†
U.S. Geological Survey,
Denver, Colorado

Open-File Report 89-573
1989

* currently, MIT, Dept. of Earth, Atmospheric, and Planetary Sciences, Earth Resources Laboratory
† Deceased.

CONTENTS

LIST OF FIGURES

LIST OF TABLES

ABSTRACT

During the summers of 1982 and 1983, a U.S.G.S. crew led by Dr. Frank Frischknecht acquired 29 magnetotelluric soundings along a profile traversing the transition zone between the Great Basin and Colorado Plateau. The profile was centered along the 36°30′ parallel, north of the Lake Mead region dividing Northwest Arizona and Southeast Nevada.

The transition zone between the Great Basin and Colorado Plateau has long been of interest because it represents active encroachment of a continental rift system into a more stable intracontinental plate. This margin is characterized geologically by rapid Cenozoic uplift, high heat flow, high conductivity and low Pn velocities.

There were two stages of processing and analysis involved in this project. After discarding unuseable stations, primarily due to equipment problems in the first summer, we were left with 18 good stations. One dimensional inversions of three or more layers were derived from these remaining stations. Secondly, the one dimensional inversions were used as starting models for two dimensional inversion and modelling. We used the data from thirteen of the stations to construct the traverse for two dimensional modelling.

This paper discusses results of inversions of the magnetotelluric soundings and their inferred relationship with the geology of the transition zone.

INTRODUCTION

The Colorado Plateau is characterized as having undergone rapid late Cenozoic uplift creating deeply incised canyons and monoclinal folding. The crust underlying the Colorado Plateau is intermediate in thickness between the stable interior plains and Basin and Range at about 35-45 km (Braile and others, 1974). General isostatic equilibrium of the Colorado Plateau yields near zero gravitational anomalies.

The Basin and Range, in contrast, represents one of the world's largest areas of intracontinental extension. The Great Basin, the northern half of the Basin and Range, is characterized by high heat flow, low P_n velocities, Quaternary and Tertiary volcanism, crust of 15-25 km thickness and thin lithosphere (Thompson and Burke, 1974) . The topography is dominated by north-south trending horst-graben sequences bounded by steeply dipping normal faults.

The transition zone between the Great Basin and Colorado Plateau is an approximately 50km wide area west of the Grand Wash Cliffs. This zone is called the Grand Wash Trough in analogy to the Wasatch Trough in Utah. The Grand Wash Trough is dominated by late Cenozoic normal faulting (Pearthree and others, 1983), high heat flow and conductivity, (Gough, 1983).

The survey the U.S.G.S. undertook extends from east to west from the Uinkaret Plateau in the Central part of the Colorado Plateau across the Hurricane Cliffs, the Shivwits Plateau and Grand Wash Cliffs through the St. Thomas Gap separating the North and South Virgin Mountains and finally onto the Mormon Mesa. This is shown in Fig. 1. A Bouguer gravity anomaly map, at a slightly different scale, is presented as Fig. 2 and shows the location

of the magnetotelluric soundings. Soundings used in the two dimensional inversion are indicated as solid circles.

GEOLOGY

Regional Geology and Geophysics

As recently as the early 1970's, the consensus of earth scientists was that the uniformly uplifted Colorado Plateau and the complexly extended Basin and Range Province were thought to be essentially independent. Looking at Fig. 2 for instance, one can see a substantial reduction in the density of gravity contours as you proceed into the Colorado Plateau. The dominant hypothesis was that a relatively isolated mantle diapir was heating the lithosphere below the Basin and Range causing it to wrench apart, this was known as the pure shear hypothesis. Another related opinion held the belief that the intrusion of large volumes of igneous rocks in vertical dikes wedged the Basin and Range apart, the wedging hypothesis.

Evidence has been presented to question these hypotheses and has caused earth scientists to rethink the tectonic processes involved in this area. The chief argument against the pure shear and the wedging hypothesis, bases on palinspastic reconstructions, are that such processes could not adequately account for the large amounts of extension present in the Basin and Range (from 60-100% or 140km,(Wernicke and others, 1982)) without a much thicker lithosphere than is geophysically evident (40 km). An explanation that could account for these observations is the recognition of the importance of low angle normal faults or detachment faults as the dominant tectonic mechanism present in the area at depth. This recognition relegates brittle, high angle normal faults to a role as antecedents of the ductile low angle normal faulting (Wernicke, 1981) .

One important consequence of the low angle normal faulting hypothesis is the definition of a discrepant zone. Wernicke (1983) defines the discrepant zone as the area where there is a deficiency in crustal thickness based on fault uplift calculations. This discrepancy is due to the thin crust created by the low angle normal faulting consuming the crust of the more stable plate. Pearthree and others (1983) showed that based on Cenozoic normal faulting, the Great Basin appears to be encroaching upon and thinning the lithosphere under the Colorado Plateau, precisely matching the definition of a discrepant zone.

Survey Specific Geology

The Uinkaret and Shivwits Plateaus which the profile traverses (Fig. 1) are comprised primarily of Paleozoic and Mesozoic sedimentary rocks. Cenozoic volcanic rocks and pediment surfaces are also present in this area. The Grand Wash Cliffs and Hurricane Cliffs are formed by steep normal faults because of rapid Cenozoic uplift and resistant limestones preventing alluvial fan development. The Northern Virgin Mountains are a faulted parallel plunging anticline and syncline metamorphic sequence of very high relief (Seager, 1970).

The Northern Virgin Mountains and the Beaver Dam Mountains to the north represent breakaway mountain ranges (Wernicke, 1983). The profile continues onto the Mormon Mesa which is a flat surface of Quaternary Alluvium.

THE MAGNETOTELLURIC SURVEY

Magnetotelluric soundings depend on ionospheric-generated currents propagating through the earth. These "telluric" currents have periods from milliseconds upward. For the lowest frequencies, with periods of greater than a day for instance, measurements must be taken from fixed geomagnetic observatories whereas the magnetotelluric method utilizes frequencies high enough so that field measurements are possible and practical. These frequencies are typically from .001 Hz to 100 Hz. The higher the frequency the less the penetration into the surface and the less volume of material that is sampled by the current. Thus the lowest frequencies of propagation are influenced by the deepest structure.

Near the surface, the flow of telluric currents is primarily controlled by electrolytic conduction through the pore fluids, as the surrounding rock matrix is essentially an insulator. Therefore, resistivity is dependent on porosity, abundance of fractures, and the salinity of the pore fluids. At depth, these pores and fractures close resulting in many fewer conduction paths and a subsequent increase in resistivity. Throughout much of the crust and often into the upper mantle, the closure of pores dominates the resistivity profile resulting in high values. Continuing deeper, dependent on the geothermal gradient, increased ionic conduction of semiconductor metallic ions due to higher temperatures dominates the resistivity profiles resulting in lower resistivities. Keeping in mind the inverse relationship between frequency and depth of investgation, an idealized magnetotelluric sounding would detect a bell-shaped curve with lower apparent resistivities at high and low frequencies and high apparent resistivities at intermediate frequencies. Because of high geothermal gradients in the transition zone and Great Basin, magnetotelluric soundings were thought capable of helping to unravel the complex geology in the transition zone.

Field measurements of magnetotelluric data require measurement of impedance, which is actually a complex tensor $Z(\omega)$, related to the resistivity-depth function. Assuming layered geometry and a horizontal surface, $Z(\omega)$ is a function of the horizontal electrical (E_x, E_y) and magnetic fields (H_x, H_y). The third component of the magnetic field (H_z) is often measured as a reference channel to detect the presence of non-layered geometry. The data are normally reduced to a complex scalar approximation of the impedance tensor comprised of an amplitude component, apparent resistivity ρ_a, and an imaginary component, phase (Vozoff, 1972).

Data Acquisition and Reduction

The U.S.G.S. has developed a portable, minicomputer based field system to measure and process magnetotelluric data real-time in the field. (Stanley and Tinkler, 1979, Stanley and Frederick, 1979). This field acquistion and processing system was used to collect the

soundings over the two field sessions.

The system uses two sets of copper sulfate electrodes separated by 150 meters to measure the electric field components (E_x, E_y). A low noise magnetometer is used to measure the magnetic field components (H_x, H_y, and H_z). Coherency, a measure of data quality, is calculated using various combinations of the above components. During the first season of field work, a cryogenic magnetometer was used but proved to be unworthy for the rugged field conditions encountered. Thus stations 1-13 had very poor coherencies due to the erratic recorded magnetic field and were unuseable. An induction coil magnetometer was used for the second field session, summer 1983, and provided much more coherent data.

While the data are collected, gains are applied and it is bandpass filtered. The data is then decimated, Fourier–transformed from the time to the frequency domain and stored for future processing all in real time.

The next step is derivation of the impedance tensor–the most important feature concerning any MT data processing system. The impedance tensor Z is a transfer function, related to the depth-resistivity relation, between the electric field E and the magnetic field H as follows, all as a function of frequency ω.

$$[E_x\ E_y] = [H_x\ H_y] \begin{bmatrix} Z_{xx} & Z_{xy} \\ Z_{yx} & Z_{yy} \end{bmatrix} \tag{1}$$

A least squares method (Swift, 1971, Vozoff, 1972, Sims and others, 1971) was used to compute the impedance tensor elements, which resulted in 4 different, useable tensor estimates for each frequency. The final estimated quantities used for this analysis consist of an apparent resistivity based on a geometric mean of the individual estimates, and an impedance phase based on an arithmetic mean. Both are computed for two directions designated as XY and YX. The orientations are determined in the tensor computations by minimizing the magnitude of the diagonal elements of the tensor, or equivalently, maximizing the off-diagonal elements. For one- and two-dimensional analysis these are resolved into a "TE mode" (assumed E-parallel to strike), and a "TM mode" (assumed E-perpendicular to strike).

Not all of the resistivities values were available for each frequency or each orientation because of some low coherencies. Resistivity values for frequencies that had coherencies less than about .87 were discarded.

Results

One Dimensional Inversions.

The one dimensional inversions were computed using a Marquardt-Levenberg algorithm (Anderson, 1979) which solves for plane wave solutions of apparent resistivities (Cagniard, 1953, Vozoff, 1972) . Input to the program is the observed response (apparent resistivity and phase) plus a starting model (a separate run for each mode, xy and yx). Output is a final model whose response is best-fitting (least squares sense) to that input, plus the computed response of the final model for visual comparison to the input response. Most of

the inversions performed were three layer inversions implying a low resistivity surface layer followed by a thick highly resistive layer and a more conductive layer at depth, forming the aforementioned bell-shaped curve. With this inversion procedure, both resistivity and depth of each layer were allowed to vary. This is advantageous because erroneous trial models will show either very low or very high resistivity layers of very large or infinitesimal thickness pointing out the need for a new starting model. Up to five layers were investigated but the best inversions were generally obtained with three layer models.

A synthesis of the best results for the one dimensional inversions, inversion solutions with three layers only, is presented as a pseudo-profile, Fig. 3, followed by the inversions in the xy, (TE) and yx, (TM) mode Fig. 4. The profile shows a thinning of the resistive upper crust westward into the Basin and Range and a nonuniform thickness for the resistive upper crust. Unfortunately, significant gaps exist in the coverage using the three layer inversion results. In these areas, inversion tried would only converge for initial models having four layers. For example, such was the case for station 24.

The inversions (Fig. 4) show the fit to apparent resistivity and phase for all stations in which it was possible to do so. Whereas the fits to resistivity are generally good, the fits to phase are not quite as precise. In general this is to be expected. It is readily apparent with the one dimensional inversions that at some stations there is a high degree of polarization evident by different resistivities in the XY and YX direction. Although purely qualitative, this "polarization" is most pronounced in stations 20,22,23,26,27 (Furgerson, 1982),28, and 30 in the Great Basin and least pronounced in stations 16,17,18 and 19 in the Colorado Plateau, Fig. 4. Station 14 in the Colorado Plateau, however, shows some polarization. Such anisotropy may be caused by near-surface contrasts, such as alluvial-bedrock contacts and imparts considerable uncertainty to 1-D interpretations

Two Dimensional Inversions.

The determination of the two dimensional structure of the transition zone was a primary objective of this report. Ted Madden and Randall Mackie of MIT, provided the code to allow us to do this. It is based on an algorithm by Swift (1971). A brief description of the procedure follows. First, the layered-earth model is approximated by a linear network of resistors with surface nodes and interior nodes. The output and input port impedances are calculated utilizing the network theorem known as Tellegen's theorem (Penfield and others, 1970) and the sensitivity matrix is evaluated using Cohn's sensitivity theorem. An efficient algorithm known as the Greenfield algorithm is employed to convolve the source properties with the resistor network (Greenfield, 1965, Swift, 1967). Once the forward model is generated, a nonlinear maximum likelihood inversion is applied to compare the data with the forward model.

The one dimensional magnetotelluric data soundings were examined to construct an optimum profile. The profile generally cut across the major strike of the transition zone which is approximately north by north east. Because of frequency coverage that did not overlap at higher frequencies between stations and low coherencies at the high frequencies, the bandwidth of the two-dimensional inversion is considerably reduced for the higher frequencies.

In fact we used thirteen periods from 6 to 152 seconds. No attempt was made in this report to interpolate the higher frequencies or constrain near surface, high frequency properties.

The specific stations used for the two-dimensional inversion were not directly adjacent to the profile so they were rotated on to the profile by tracing gravity contours. For the most part, the profile cut across the strike of the geology so the rotation by tracing gravity contours just involved offsetting the station along a line perpendicular to the profile, either north or south. But particularly in the Virgin Mountains area the geology was so complex as shown by the gravity contours Fig. 2 that the stations were offset to the west when plotted on the profile line.

Many orders of magnitude differences in resistivity are possible over a few kilometers. To relax the fit of the inversion procedure, dummy nodes were interspersed in between real stations when constructing the resistor network such that no two real stations were adjacent.

Polarization is an important consideration in the inversion process. The programs we used assumed E perpendicular to strike and because the profile was constructed perpendicular to the major strike of the transition zone this assumption is valid. If this assumption is violated the data need to be rotated. No attempt was made to rotate the data in this report. The YX orientation as shown in the 1-D inversions was used.

Again, Fig. 2 shows the location of each station superimposed on a gravity base map. The profile included stations 17, 16, 14, 15, 18, 24, 22, 27, 23, 21, 20, 31, and 30, proceeding from east to west. These stations are delineated by circles in Fig. 2.

The largest challenge encountered in implementing a two dimensional inversion for magnetotelluric data is the problem of nonuniqueness. Specifically, with this type of data set, a large variety of models could properly model the data.

In particular, three models were attempted and refined based on the one dimensional inversion results, the inferred geology and the convergence and divergence properties of the models as modelling proceeded. The first model incorporated a highly resistant layer below the Colorado Plateau and at depth a less resistive layer. At the surface, a low resistivity layer was assumed. This model was designated the "Crustal" model although it's important to remember that these highly resistive zones do not specifically correlate with crustal thicknesses. The second model was the "No Crust" model and has resistivities not including a highly resistive zone. The third model, is highly speculative but we were led to it on the basis of the inversion results. It is called the "Window" model because of a very low resistivity "Window" from the surface to depth in the Great Basin.

Initial attempts at the inversion yielded profiles which did not contain the highly resistive layer and the data did not seem amenable to inserting a highly resistive layer. For example, any attempt at inserting a highly resistive layer in the initial model would meet with the inversion procedure acting erratically and pushing the depth to infinity or the thinness to zero of these layers. However, carefully and with many different inversion attempts, a resistive layer was inserted until the final inversion fit the data almost as well as the inversions without a resistive layer. This profile is plotted in Figure 5 and the contours are gentle and interpretable.

Model	RMS Error	Right Hand Side Error
"Crustal" Model	28.4	2.2
"No Crust" Model	27	2.4
"Window" Model	20	6.0

Table 1 -- Comparison of RMS and Right Hand Side Errors for the three input models

Next the inversion was tried without an added resistive layer. The results are displayed in Fig. 6. This provided a better fit, however the contours are less smooth than the "Crustal" model and more likely to be mathematical artifacts.

Finally, a model suggested by the inversion procedure was used, Fig. 7, the "Window" model. This model featured a low resistivity "window" or conduit into the lower crust adjacent to the Virgin Mountains. This model had the lowest rms (root mean squared) error, decreasing from 26% to 20%. Table 1 below shows this decrease in error. Fig. 8 shows that this decrease in error is chiefly through much better fits to the phase response. The right hand side error is an indication of the convergence properties of the inversion. Both the values at 2 and 6 percent are very good. Still this model is highly speculative and more data would need to be taken to ascertain whether this is a real phenomena or an artifact of the inversion process.

Plots for the resistivity and phase data for each station along with the responses from the three different models are shown in Fig. 8. The series of plots proceeds from bottom to top corresponding to westernmost to easternmost stations.

Essentially, what these results tell us is that the frequencies in this survey are not necessarily low enough to adequately delineate a lower highly resistive layer, if there is one. If lower frequency data was present we could begin to compare these results with the thesis work of Swift in Arizona showing typical conductivity profiles (Swift, 1967) . All three models show the dramatic increase of resistivity into the Colorado Plateau and also show that the boundary dips into the Colorado Plateau.

CONCLUSIONS

The results of this study would seem to support the hypothesis that the transition zone between the Colorado Plateau and Great Basin is not as distinct at depth as it is at the surface. This is confirmed by the results for both the one dimensional and two dimensional inversions studied here. At the surface, the Grand Wash Cliffs delineate the transition zone but at depth a highly resistive layer indicated by the "Crustal" model thickens into the Colorado Plateau.

There is a dramatic difference in magnitudes of resistivites when traversing from the Plateau to the Basin, often as much as two or three orders of magnitude. Secondary features such as surface or buried metamorphics also affect these results (Jiracek and others, 1983) . Although qualitative, the transition into the Great Basin also shows an increase in polarization.

The chief limitation of this data set is the limited bandwidth and the incomplete spectrum. This is partially due to the difficulty of achieving good coherencies and good data acquisition with the low frequencies. We believe these areas are important to study with magnetotelluric soundings but lower frequency data needs to be investigated. A second limitation was that stations needed to be traced along gravity contours to construct the profile. In the Colorado Plateau, this was a simple correction along strike, but this action became much more speculative in the Virgin Mtns area. It would be preferable to run this survey, or a survey in a similar area, with a straight line cross-section profile as an objective.

An interesting and speculative model best fit the data for the two dimensional inversion results. This model provided a "window" into depth that had very low resistivity. RMS error was dramatically reduced with this model. Partially due to the lack of uniqueness and limited bandwidth it is not known whether this is might be an area of crustal thickness deficiency, an artifact of inversion, or a wrong answer.

ACKNOWLEDGEMENTS

This paper is dedicated to the memory of Frank Frischknecht who unfortunately fell prey to a tragic accident while working for the USGS. We would like to acknowledge Dal Stanley of the USGS for providing the data processing system used in this paper. Also, Walt Anderson of the USGS, wrote the one dimensional inversion software used in this report. We would like to thank Ted Madden and Randall Mackie for providing us with the two dimensional network inversion program and providing good advice on the procedures of 2D inversion. We would also like to thank Doug Klein and David Fitterman of the USGS for extremely constructive reviews.

REFERENCES

Anderson, W.L., 1979, Program IMSLPW: Marquardt inversion of planewave frequency soundings: U.S. Geological Survey Open File Report 79-586, U.S. Geological Survey

Braile, L.W., Smith, R.B., Keller, G.R., Welch, R.M., and Meyer, R.P., 1974, Crustal structure across the Wasatch front from detailed seismic refraction studies: J. Geophys. Res., v. 79, p. 2669–2677.

Cagniard, L., 1953, Basic theory of the magneto-telluric method of geophysical prospecting: Geophysics, v. 18, p. 605–635.

Gough, D.I., 1983, Electromagnetic geophysics and global tectonics: J. Geophys. Res., v. 88, p. 3367–3377.

Greenfield, R.J., 1965 Two-dimensional calculations of magnetic micropulsation resonances: PhD thesis, Mass. Inst. of Tech.

Lysonski, J.C., Aiken, C.L.V., and Sumner, J.S., 1981, The complete residual Bouguer gravity anomaly map, Grand Canyon: U.S. Dept. of Energy, 1981.

Lysonski, J.C., Aiken, C.L.V., and Sumner, J.S., 1981, The complete residual Bouguer gravity anomaly map, Las Vegas: U.S. Dept. of Energy, 1981.

Pearthree, P.M, Menges, C.M. and Mayer, L., 1983, Distribution, recurrence, and possible tectonic implications of late Quaternary faulting in Arizona: Open File Report 83-20, State of Arizona Bureau of Geology and Mineral Technology.

Penfield, P., Jr., Spence, R., and Duinker, S., 1970, Tellegen's theorem and electrical networks: M.I.T. Press, 1970.

Seager, W.R., 1970, Low-angle gravity glide structures in the Northern Virgin Mountains, Nevada and Arizona: Geol. Soc. Am. Bull., v. 81, p. 1517–1538.

Sims, W.E., Bostick, F.X., Jr., and Smith, H.W., 1971, The estimation of magnetotelluric impedance tensor elements from measured data: Geophysics, v. 36, p. 938–942.

Stanley, W.D. and Frederick, N.V., 1979, A real-time MT system: U.S. Geological Survey Open-File Report 79-R27, U.S. Geological Survey

Stanley, W.D., and Tinkler, R.W., 1979, A low cost, low noise, practical magnetotelluric coil system: U.S. Geological Survey Open-File Report 83-0085, U.S. Geological Survey

Swift, C.M., Jr., 1967, A MT investigation of an electrical anomaly in the SW United States: PhD thesis, Mass. Inst. of Tech.

Swift, C.M., Jr., 1971, Theoretical magnetotelluric and turam response from two-dimensional inhomogeneities: Geophysics, v. 36, p. 38–52.

Thompson, G.A., and Burke, D.B., 1974, Regional geophysics of the Basin and Range Province: Earth Planet. Sci. Annu. Rev., v. 2, p. 213–238.

Vozoff, K., 1972, The magnetotelluric method in the exploration of sedimentary basins: Geophysics, v. 37, p. 98–141

Wernicke, B., 1981, Low-angle normal faults in the Basin and Range province: nappe tectonics in an extending orogen: Nature, v. 291, p. 645–647.

Wernicke, B., 1983, Uniform-sense normal simple shear of the continental lithosphere: Can. J. Earth Sciences, v. 22, p. 108–125.

Wernicke, B., Spencer, J.E., Burchfiel, B.C., and Guth, P.L., 1982, Magnitude of crustal extension in the Southern Great Basin: Geology, 10:499–502, 1982.

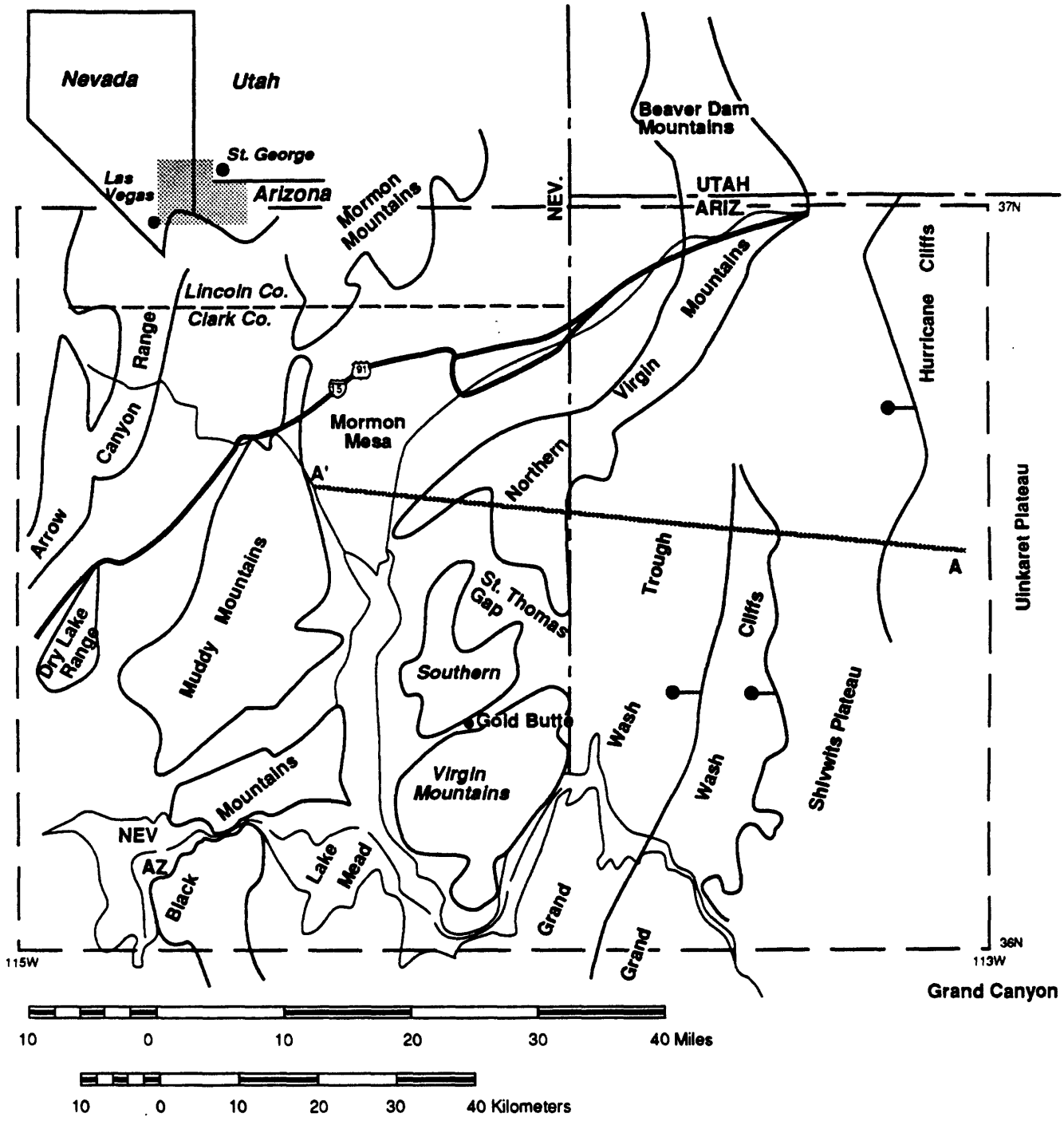

Fig. 1 -- Base geologic map modified from Seager, 1970. The magnetotelluric profile is along line A-A' and the gravity map portrayed in Fig. 2 is shown as a dashed outline.

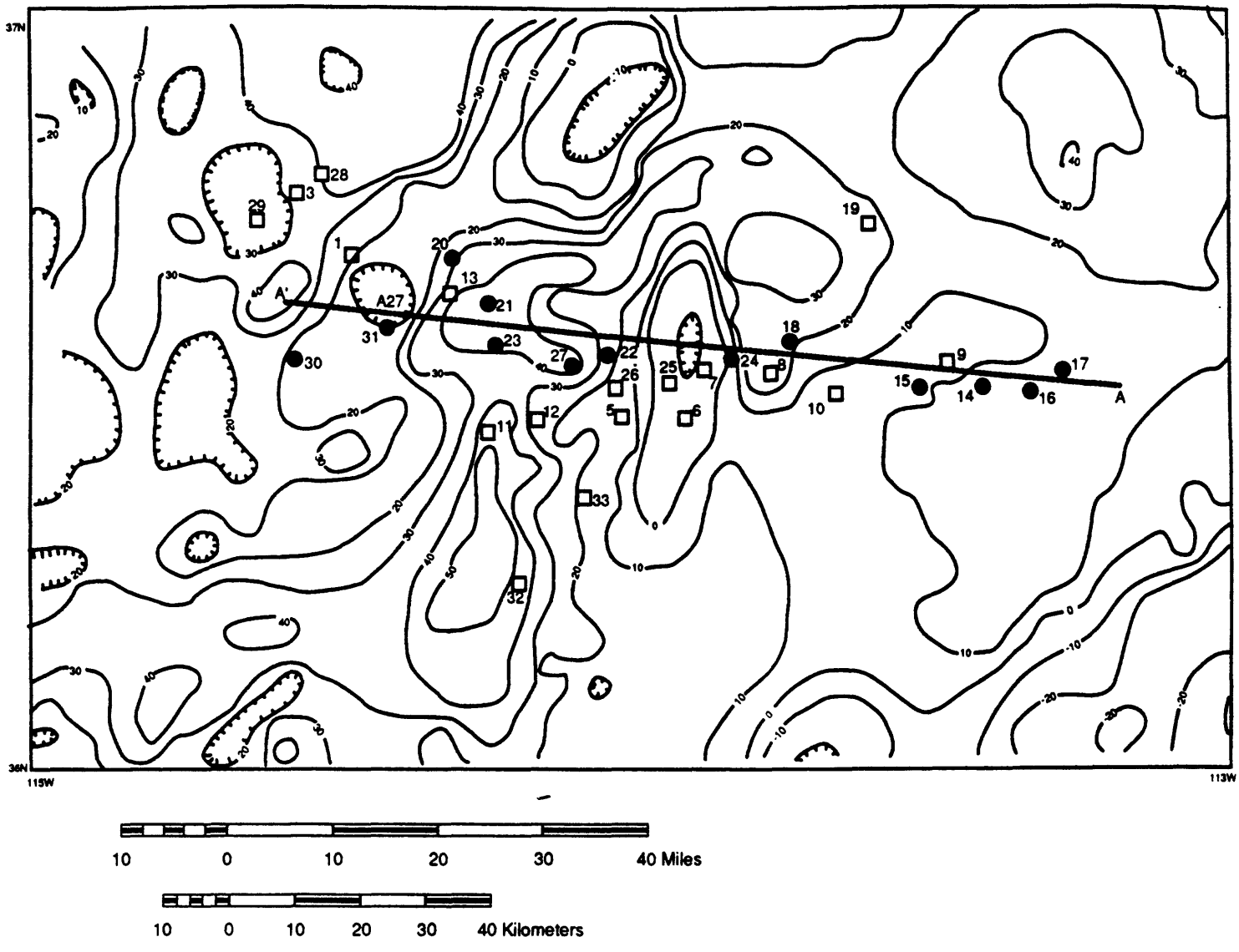

Fig. 2 -- Combined gravity contours from the 1:250,000 Complete Residual Bouguer Gravity Anomaly Maps, Las Vegas and Grand Canyon Sheet. (Lysonski et. al., 1981a, 1981b). Superimposed are magnetotelluric station locations and traverse used for two dimensional profile. Stations denoted by circles were used to construct the traverse.

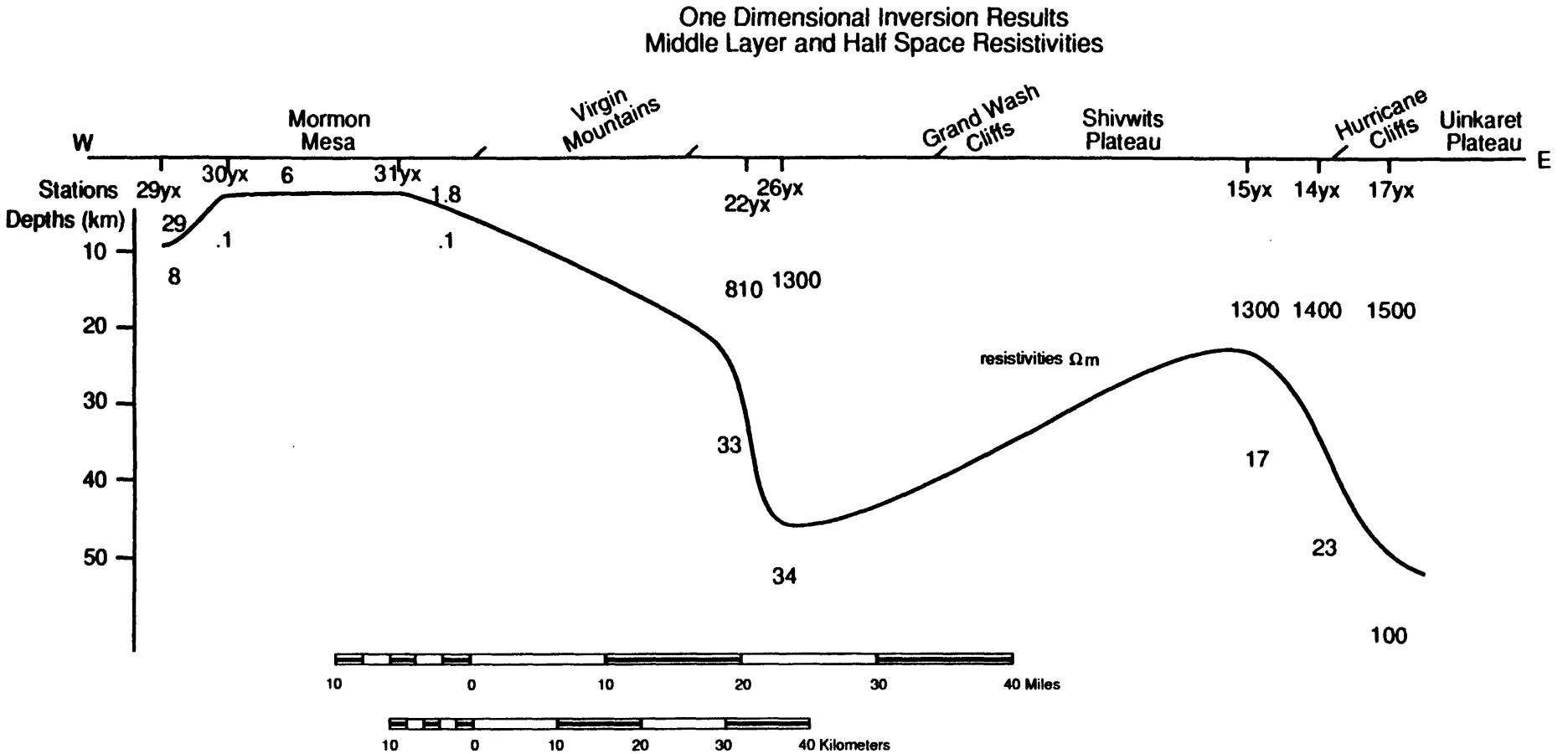

Fig. 3 -- Composite profile results of one dimensional inversions. This line parallels that for the traverse for the two dimensional inversions. Station designation include the orientation (yx or xy) of the tensor response component whose 1-D inversion was selected for compositing.

Station 14 - 1D Inversions

XY Polarization

km	
.5	23 Ω m
13.7	130000 Ω m
	13 Ω m

YX Polarization

km	
.02	3 Ω m
36.2	1400 Ω m
	23 Ω m

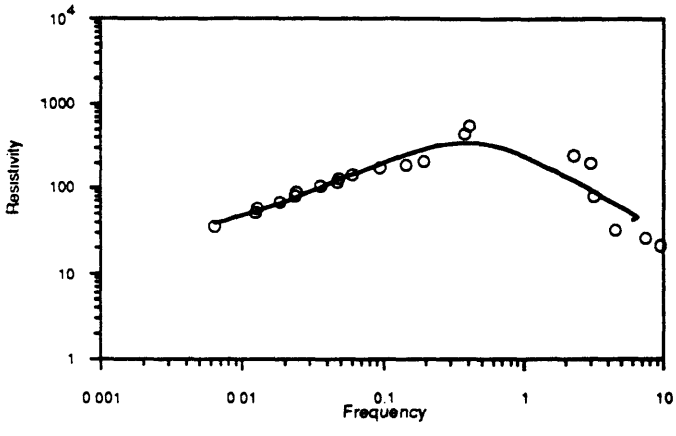

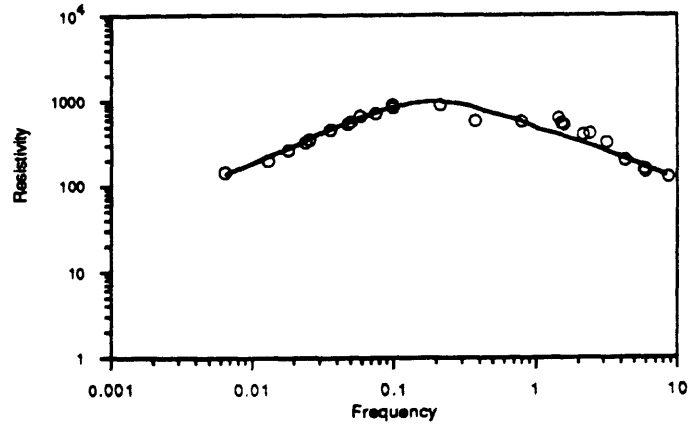

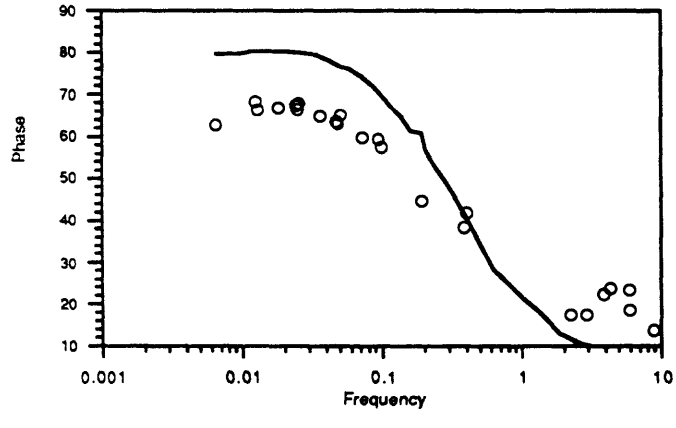

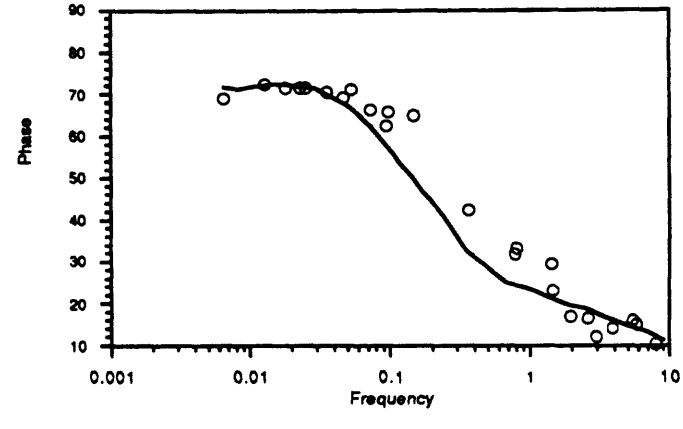

Fig. 4 -- One dimensional inversions, this page and succeeding pages show xy and yx polarizations. Both data and inversion result are plotted on the same graph for resistivity and phase respectively, Abscissa is frequency.

Station 15 - 1D Inversions

XY Polarization

km	
.1	11 Ω m
21	1300 Ω m
	17 Ω m

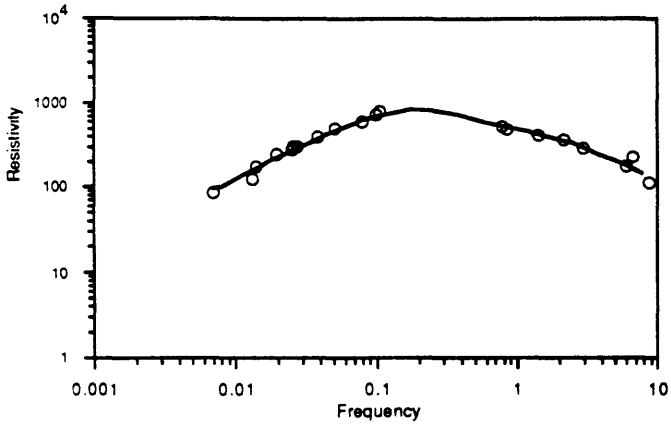

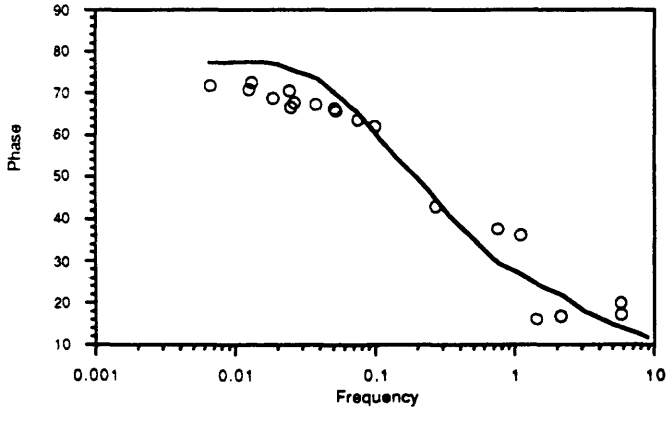

YX Polarization

km	
.1	1.4 Ω m
24.3	1300 Ω m
	17 Ω m

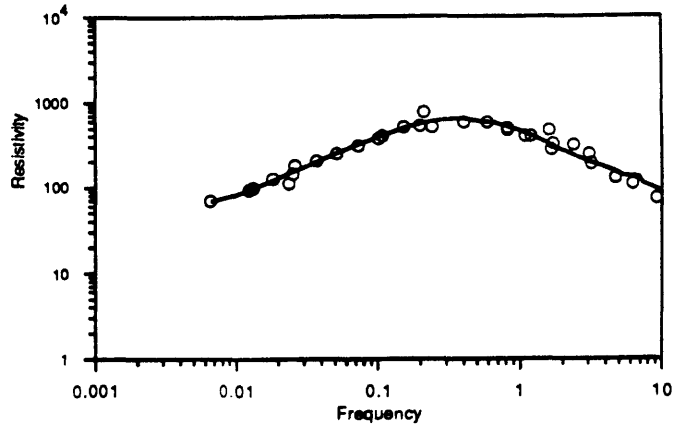

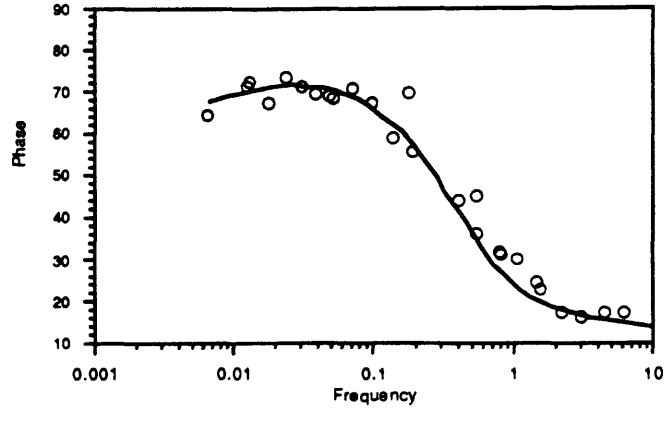

Station 16 - 1D Inversions

XY Polarization

km	
.6	56 Ω m
13	9800 Ω m
51	510 Ω m
	37 Ω m

YX Polarization

km	
.6	57 Ω m
14	38000 Ω m
38	450 Ω m
	10 Ω m

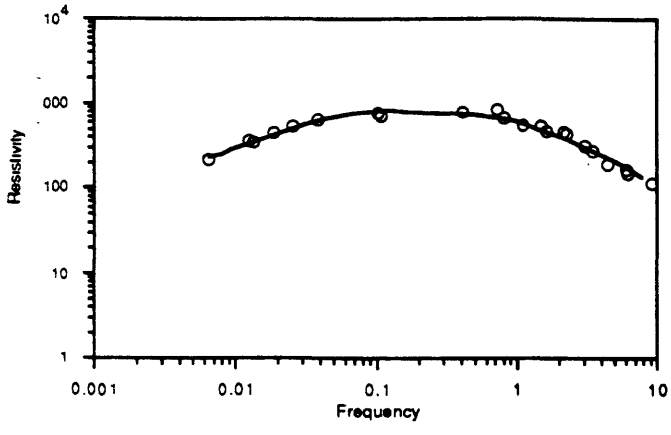

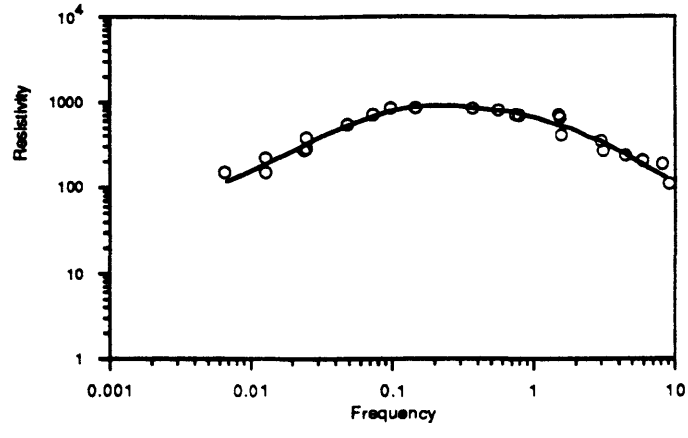

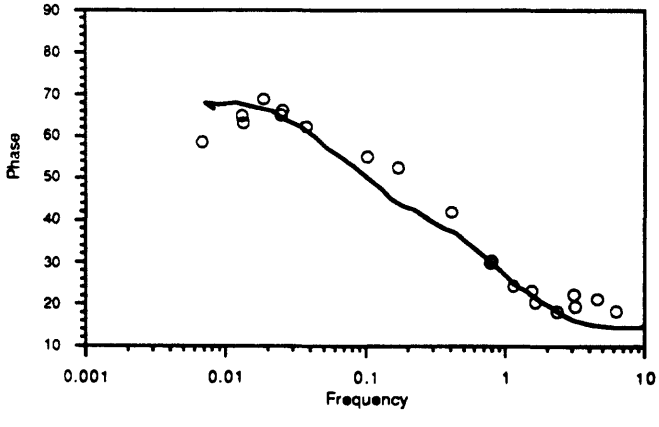

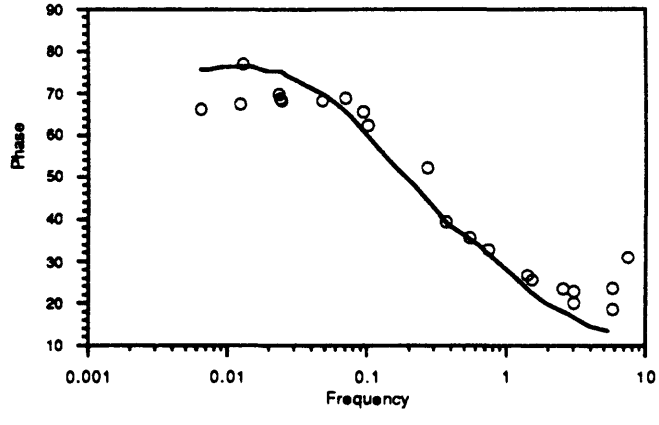

Station 17 - 1D Inversions

XY Polarization

km	
.6	75 Ω m
6.4	3500 Ω m
46	1500 Ω m
	80 Ω m

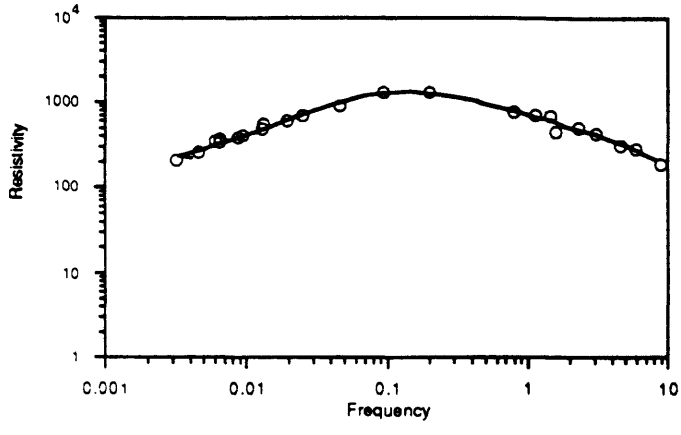

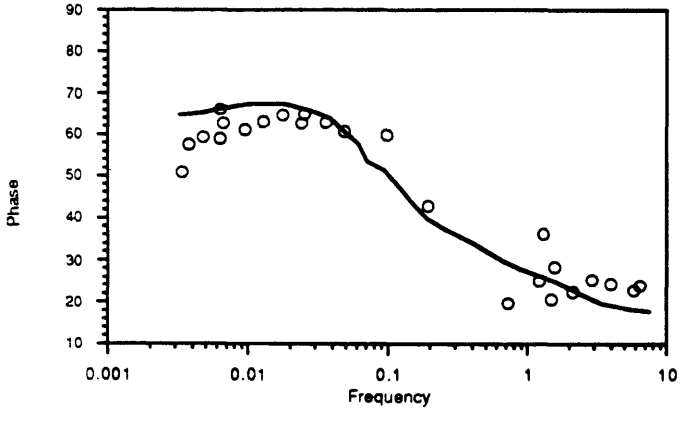

YX Polarization

km	
.1	21 Ω m
49	1400 Ω m
	70 Ω m

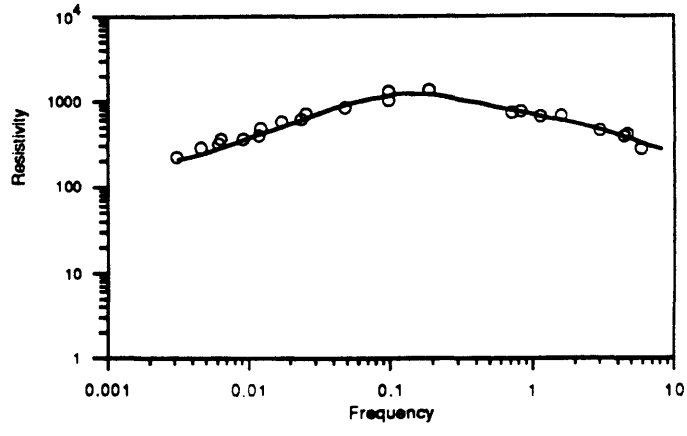

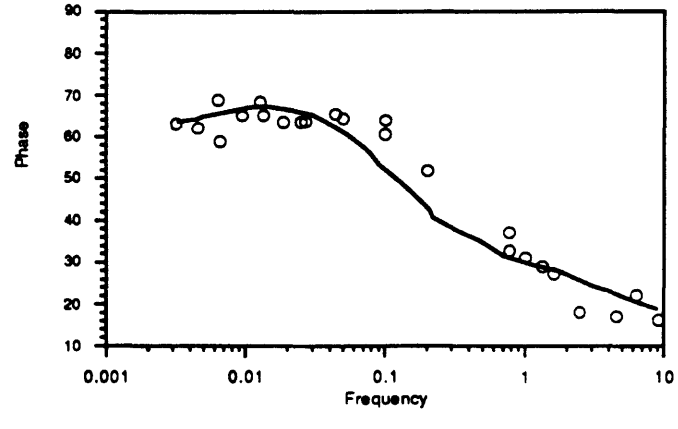

Station 18 - 1D Inversions

XY Polarization

km	
.1	18 Ω m
26	1500 Ω m
	41 Ω m

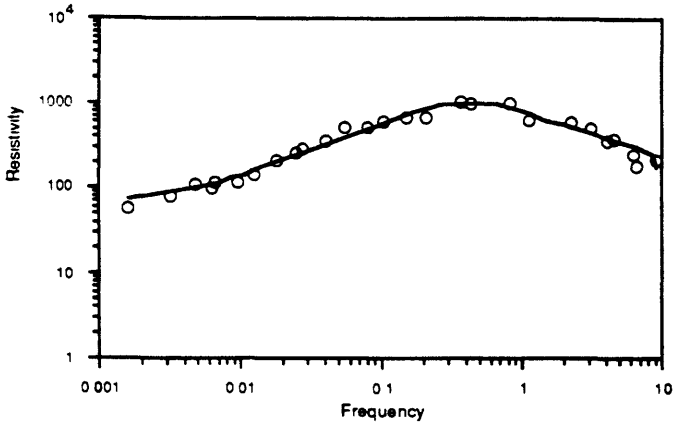

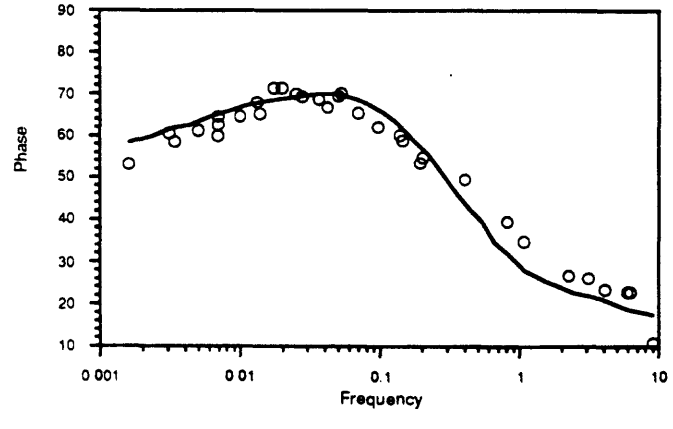

YX Polarization

km	
.46	31 Ω m
21	1100 Ω m
	20 Ω m

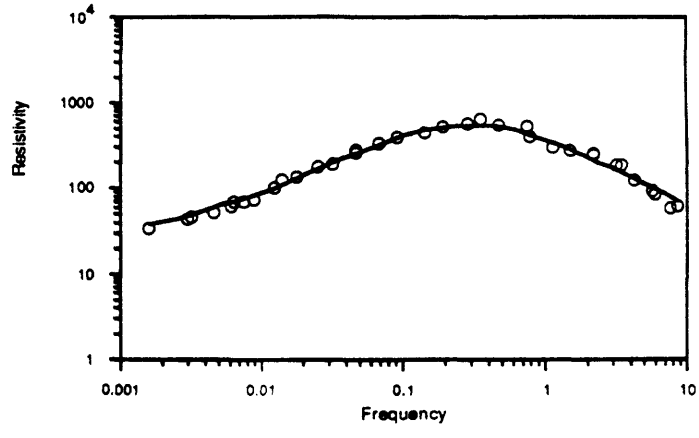

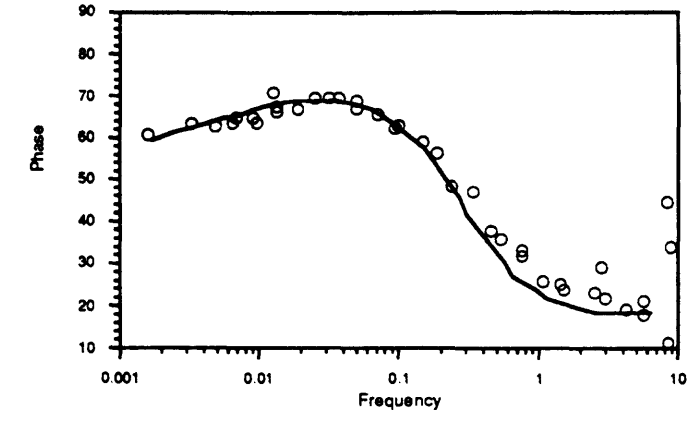

Station 19 - 1D Inversions

XY Polarization

km	
.8	100 Ω m
7.3	44000 Ω m
45	1300 Ω m
	16 Ω m

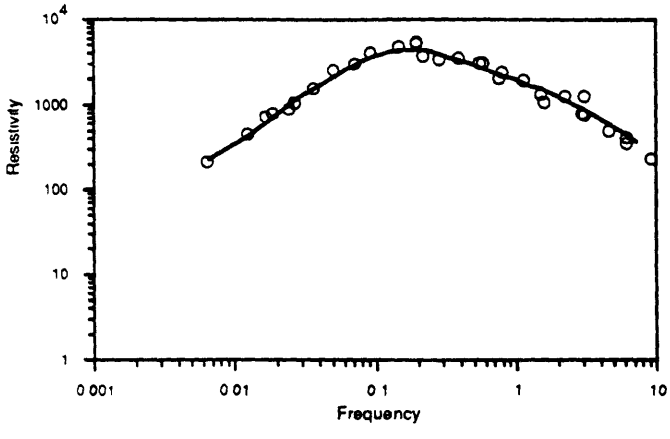

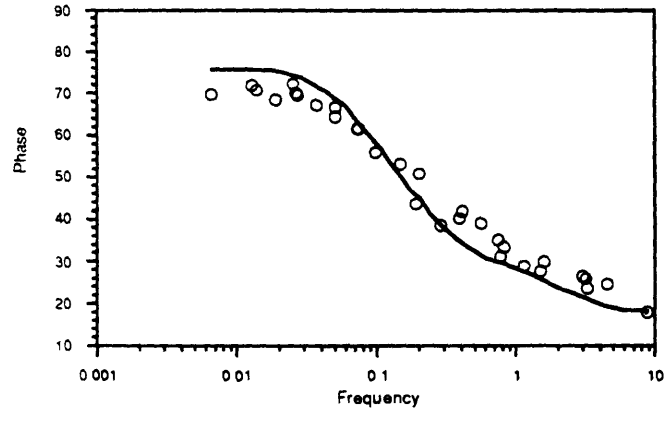

YX Polarization

km	
.07	1.5 Ω m
41	1430 Ω m
	23 Ω m

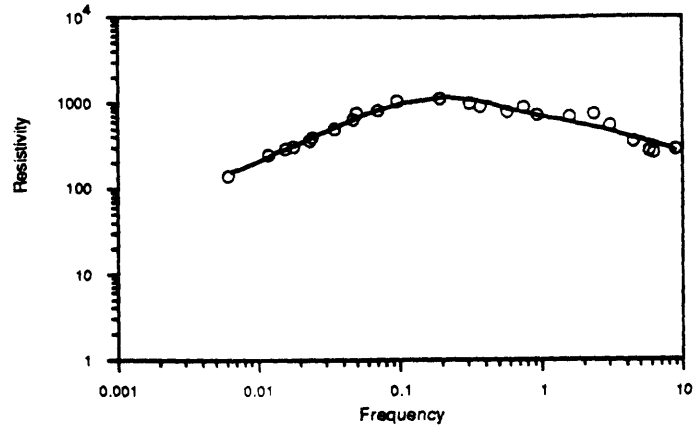

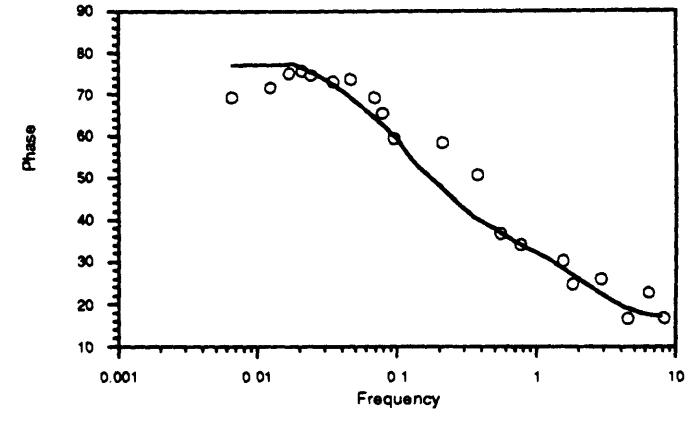

Station 20 - 1D Inversions

XY Polarization

km	
.2	6 Ω m
12	41 Ω m
	1.9 Ω m

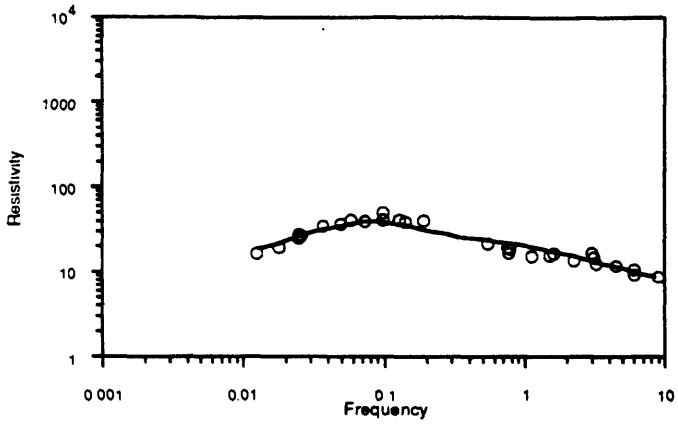

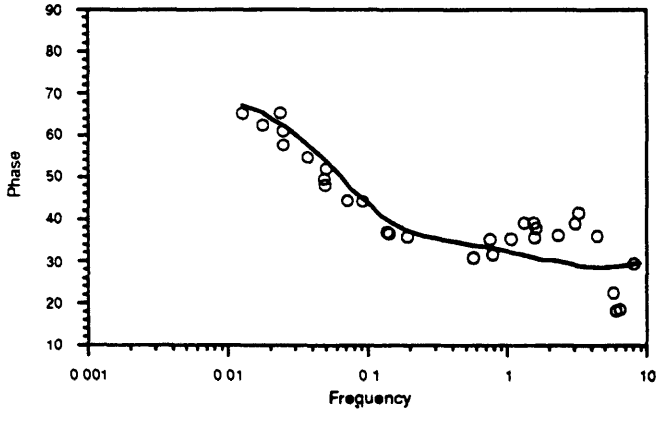

YX Polarization

km	
.002	.1 Ω m
3.6	14 Ω m
	1.3 Ω m

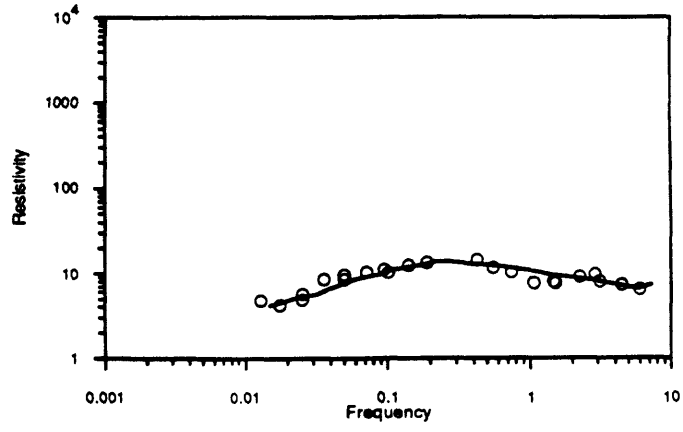

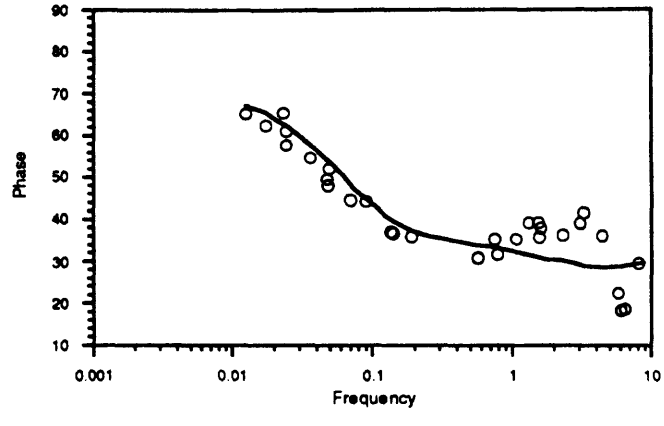

Station 21 - 1D Inversions

XY Polarization

km

.04 — 6 Ω m

26 — 580 Ω m

.1 Ω m

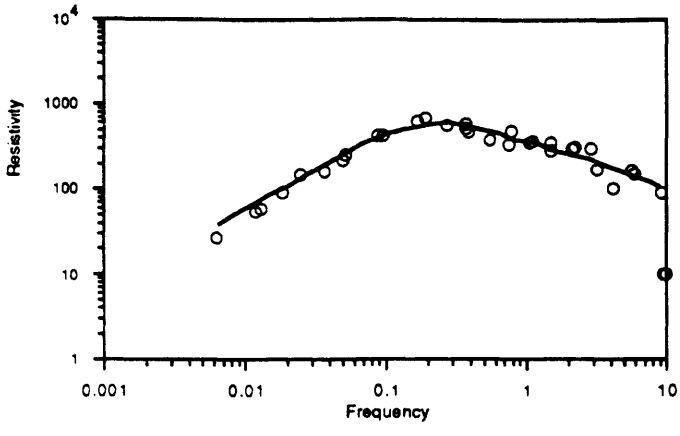

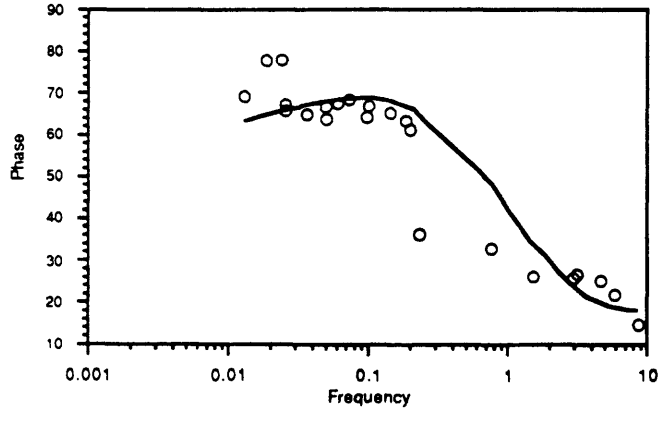

YX Polarization

(unknown)

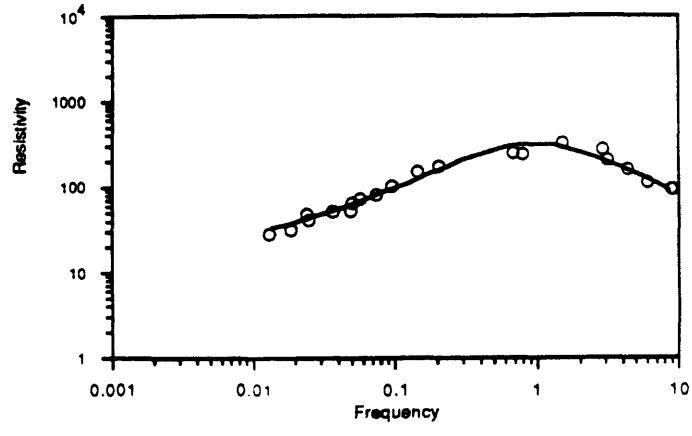

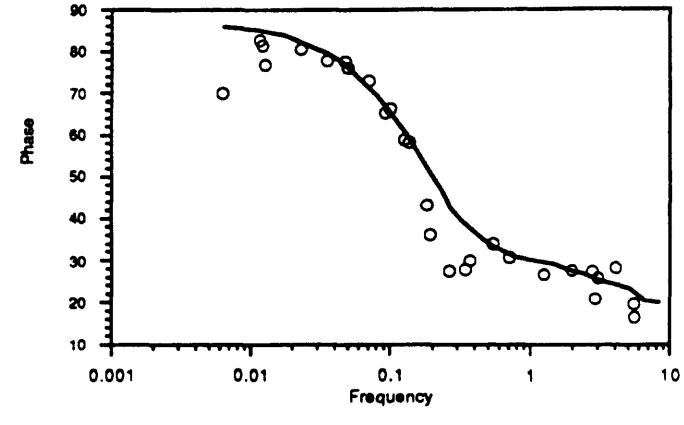

Station 22 - 1D Inversions

XY Polarization

km	
.002	.3 Ω m
12	160 Ω m
	4.2 Ω m

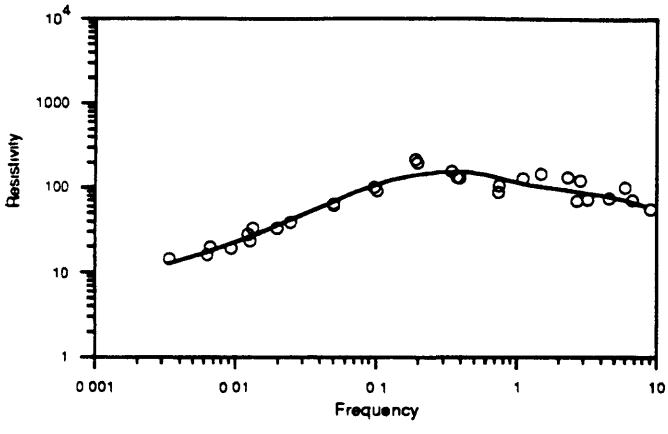

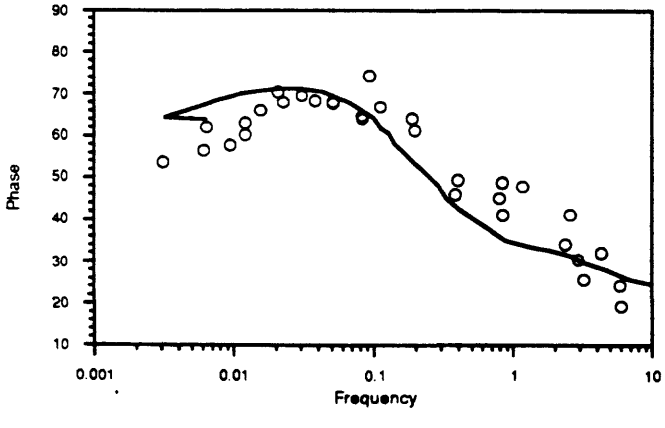

YX Polarization

km	
.07	9 Ω m
24	810 Ω m
	32 Ω m

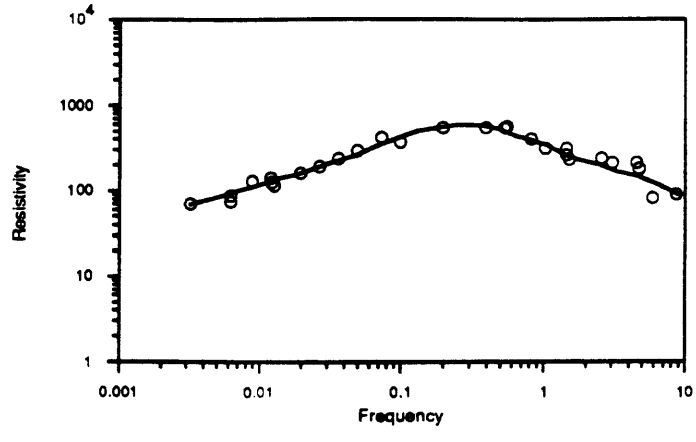

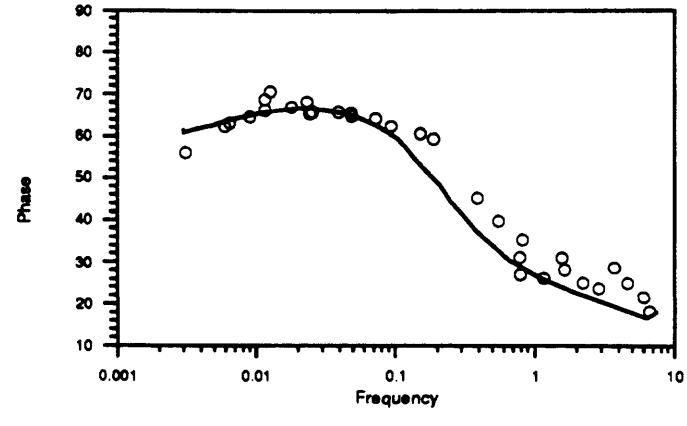

Station 23 - 1D Inversions

XY Polarization

km	
	45 Ω m
3.4	
	200 Ω m
4.4	
	.5 Ω m

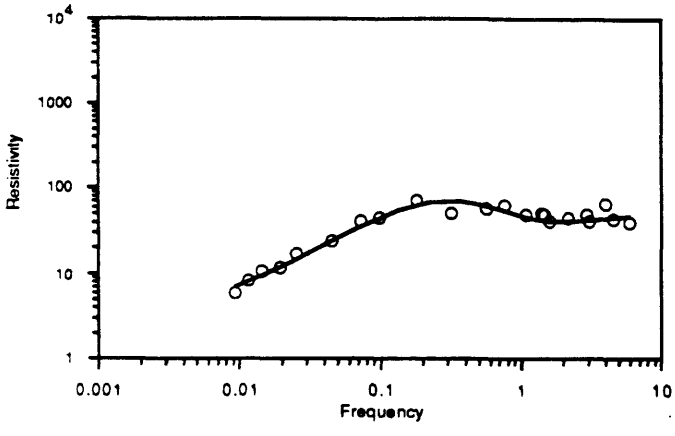

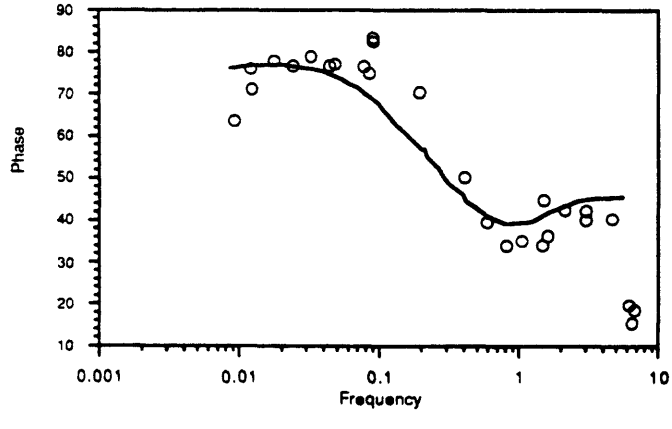

YX Polarization

km	
	8 Ω m
.09	
	63 Ω m
6.8	
	9800 Ω m
15	
	4.6 Ω m

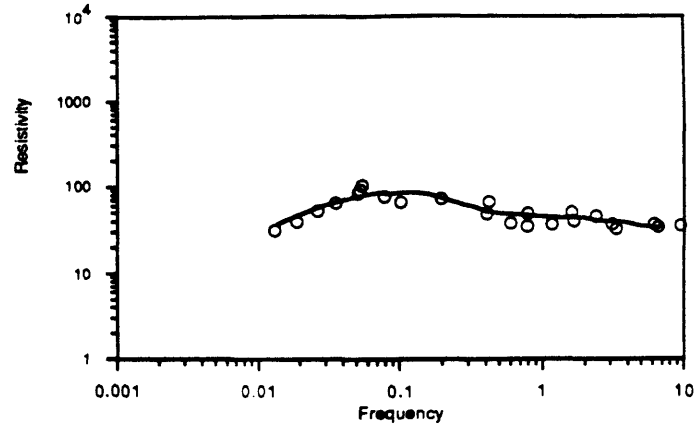

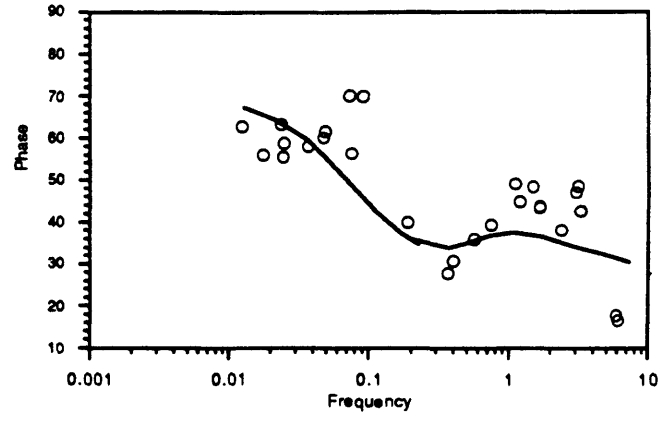

Station 24 - 1D Inversions

XY Polarization

km	
.04	3.1 Ω m
1.3	62 Ω m
9.3	26 Ω m
	1.1 Ω m

YX Polarization

km	
.8	20 Ω m
.8	2200 Ω m
3	8.0 Ω m
	.8 Ω m

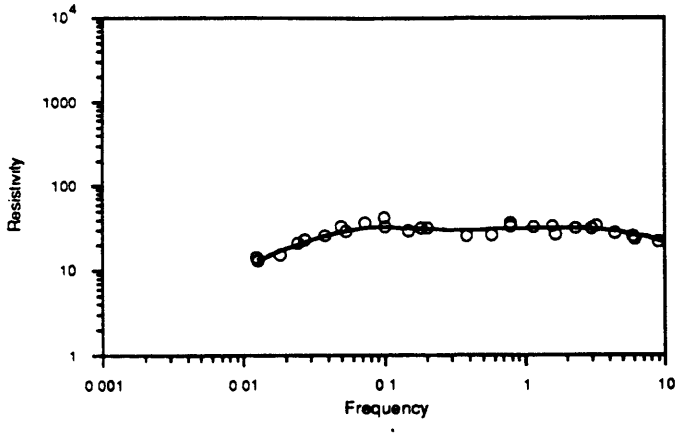

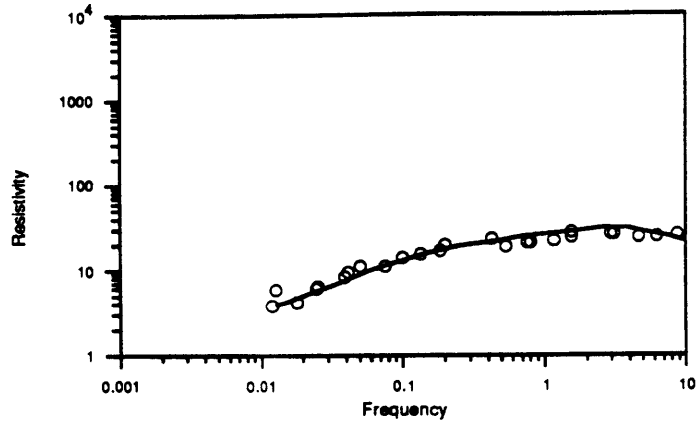

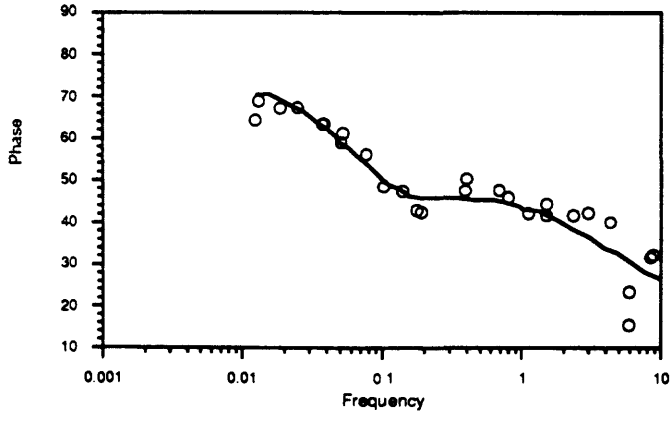

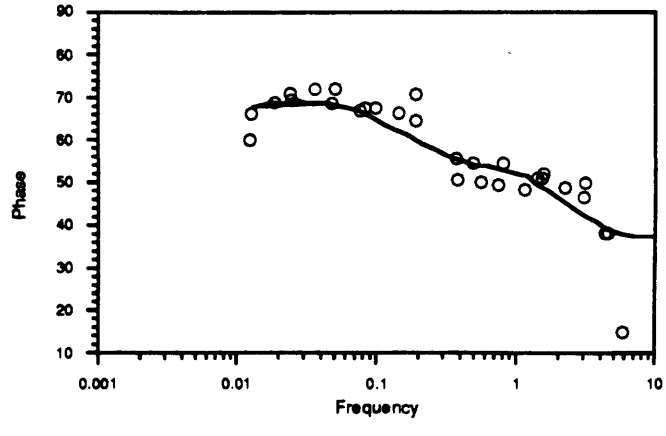

Station 25 - 1D Inversions

XY Polarization

km	
.21	5.0 Ω m
1.2	8100 Ω m
.1	.6 Ω m
7.4	1200 Ω m
	2 Ω m

YX Polarization

km	
.005	.2 Ω m
1.2	9500 Ω m
1.4	1.9 Ω m
	.2 Ω m

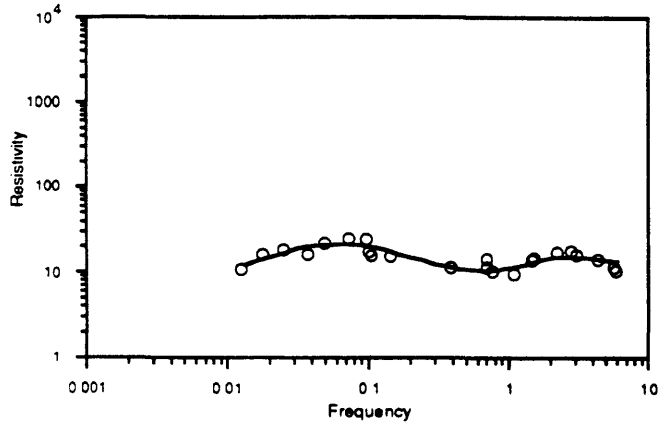

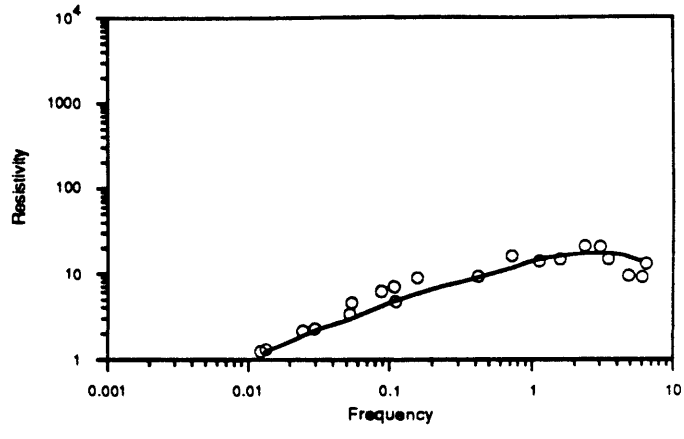

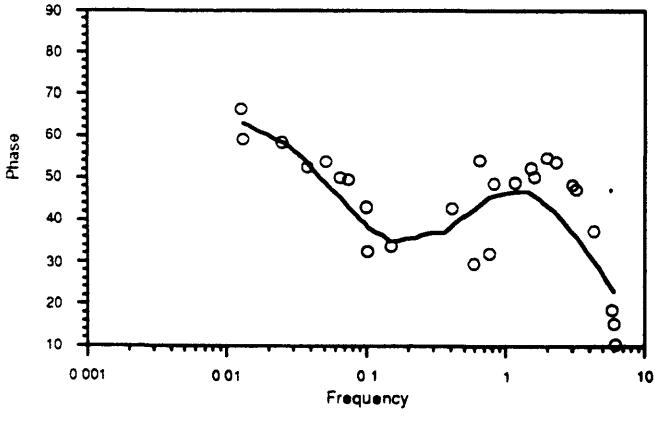

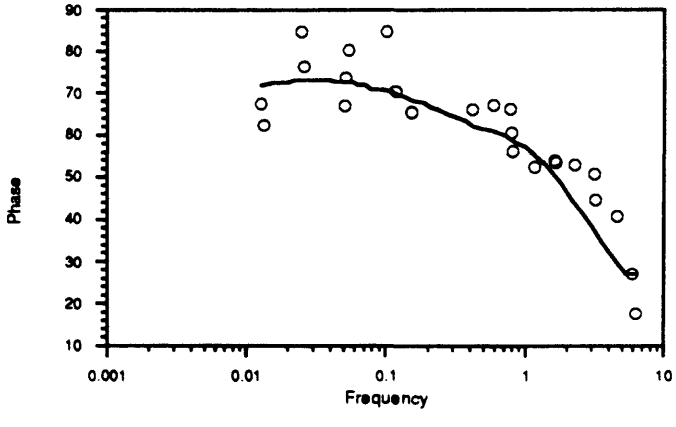

Station 26 - 1D Inversions

XY Polarization

km	
.001	.1 Ω m
8.3	61 Ω m
	3.7 Ω m

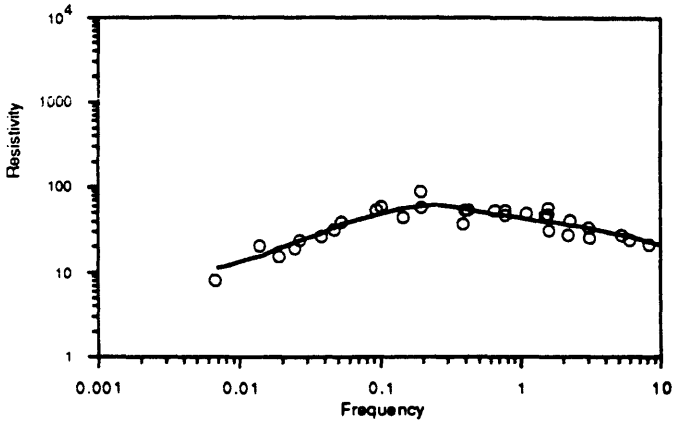

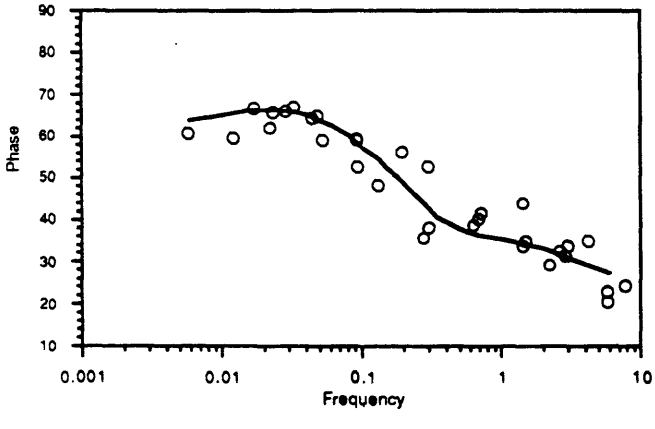

YX Polarization

km	
.07	.2 Ω m
24	1300 Ω m
	34 Ω m

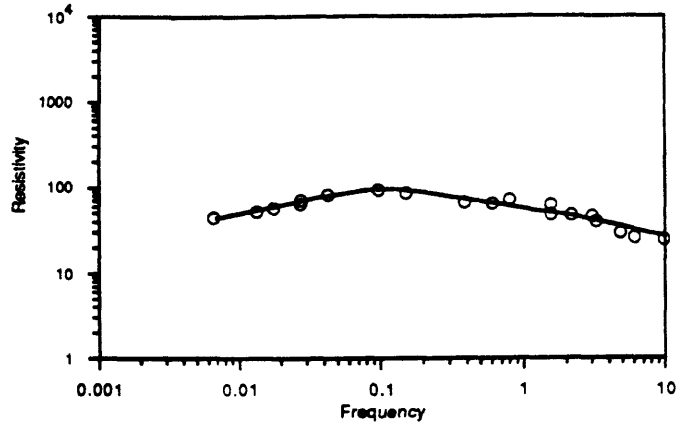

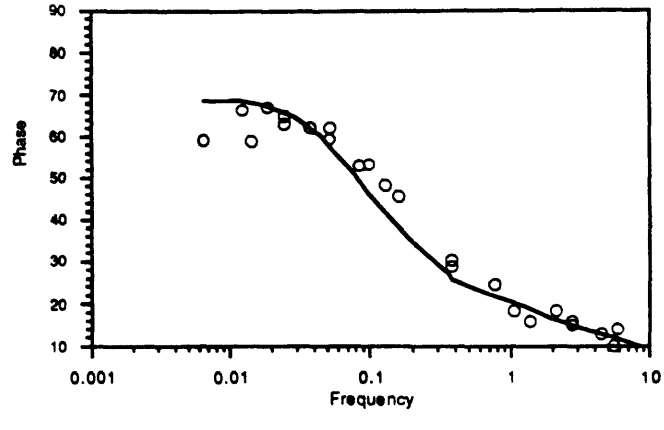

Station 27 - 1D Inversions

XY Polarization

km	
.23	50 Ω m
4.6	5900 Ω m
28	600 Ω m
	66 Ω m

YX Polarization

km	
.02	7.8 Ω m
87	6700 Ω m
	270 Ω m

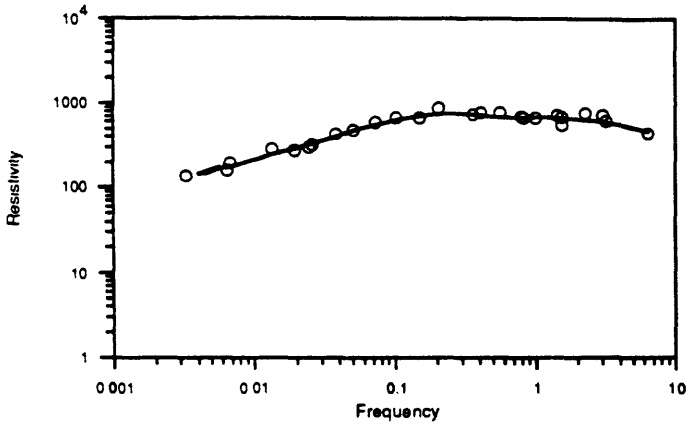

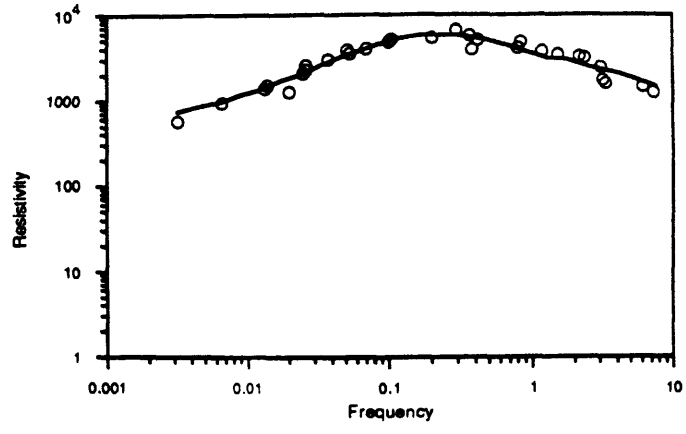

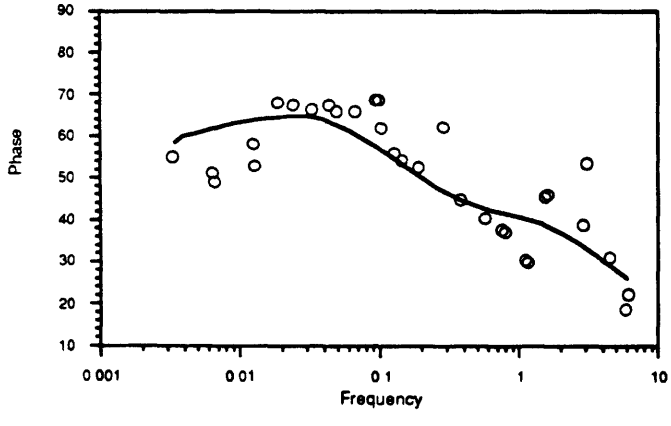

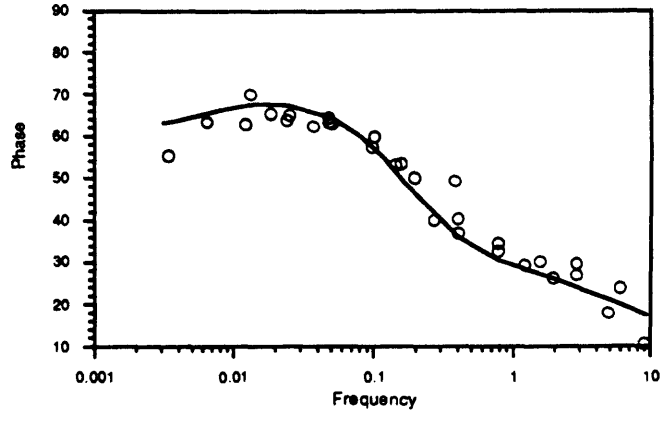

Station 28 - 1D Inversions

XY Polarization

km	
3.7	9.9 Ω m
52	.02 Ω m
	168 Ω m

YX Polarization

km	
1.6	52 Ω m
21	190 Ω m
	3 Ω m

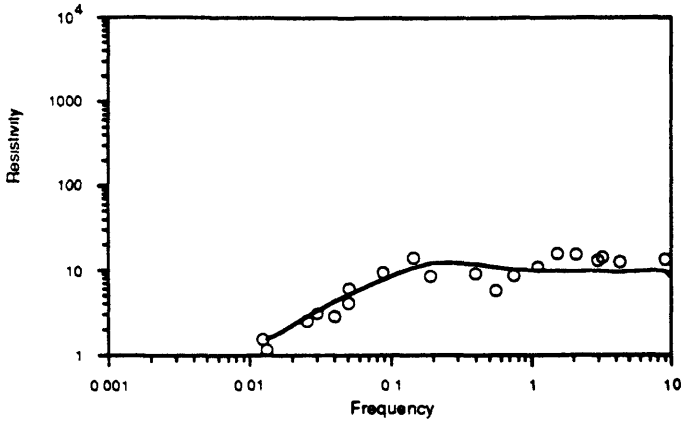

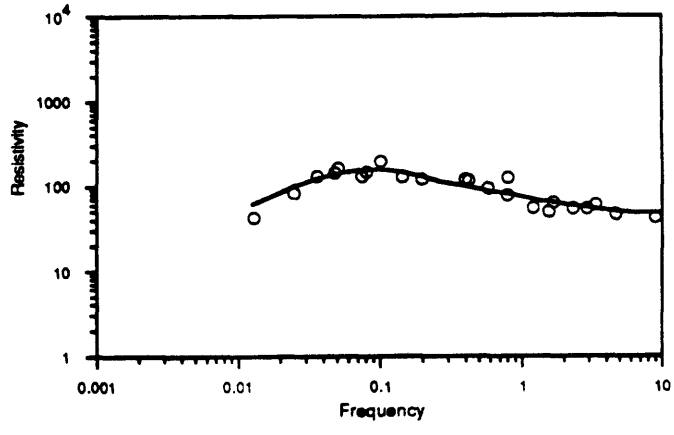

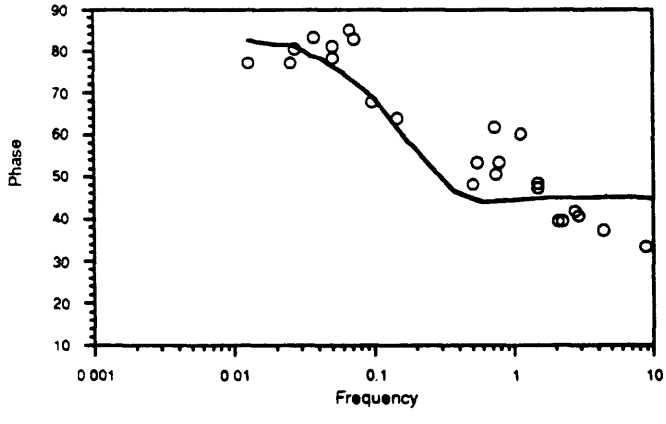

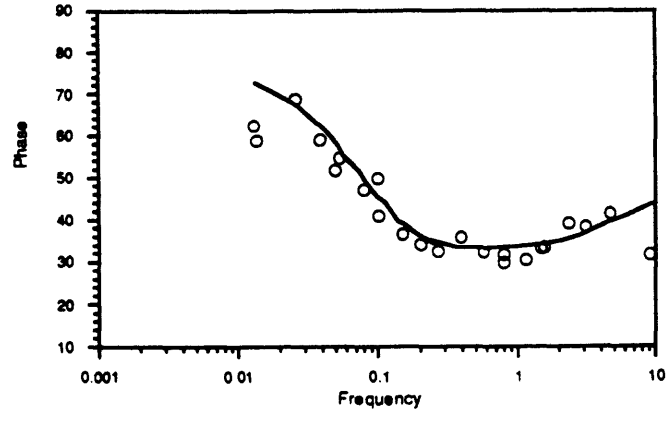

Station 29 - 1D Inversions

XY Polarization

km	
.44	5.2 Ω m
9.7	67 Ω m
	3.7 Ω m

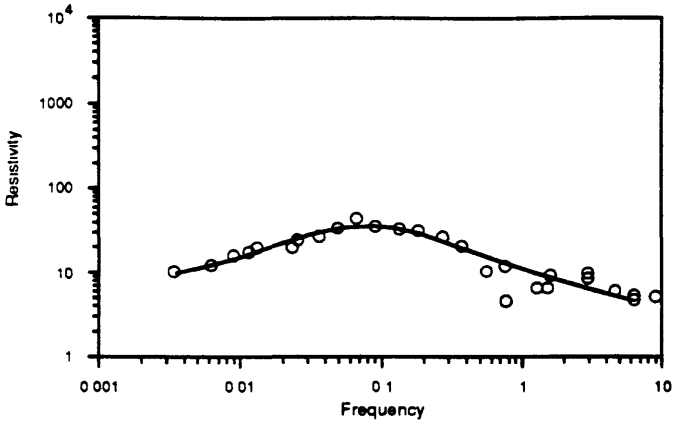

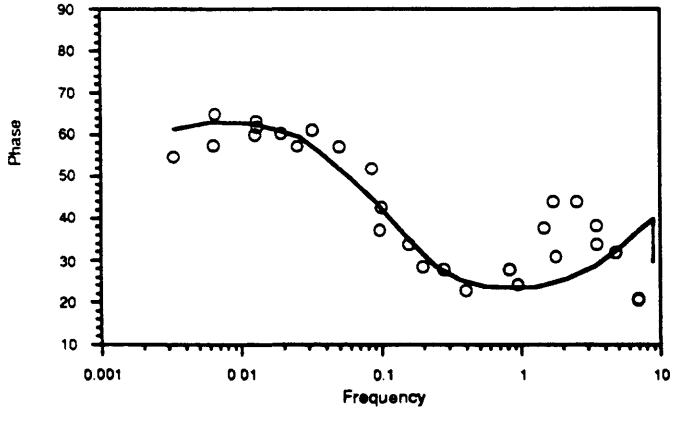

YX Polarization

km	
.3	5.1 Ω m
9.2	29 Ω m
	9 Ω m

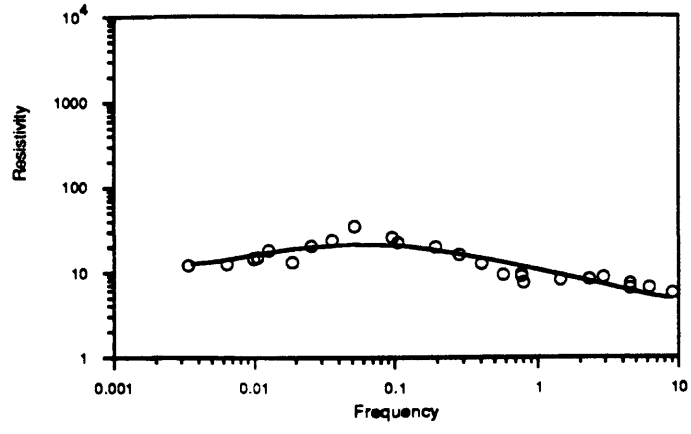

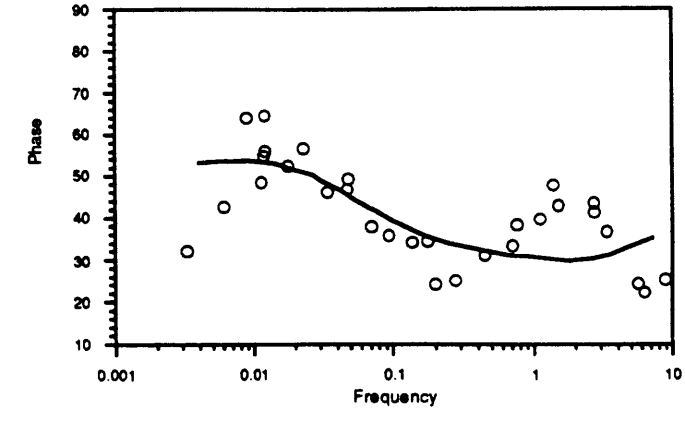

Station 30 - 1D Inversions

XY Polarization

km	
.1	5 Ω m
8.4	30 Ω m
	1.7 Ω m

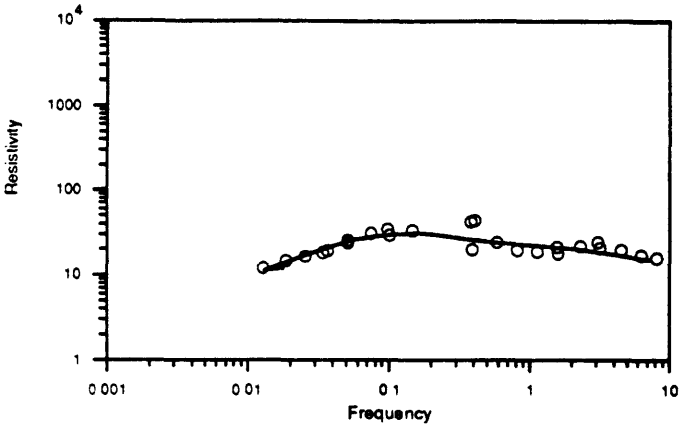

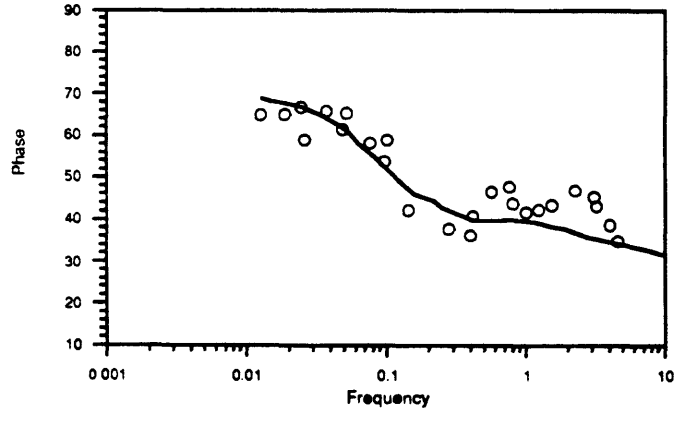

YX Polarization

km	
.08	6.9 Ω m
.6	600 Ω m
3	6.0 Ω m
	.1 Ω m

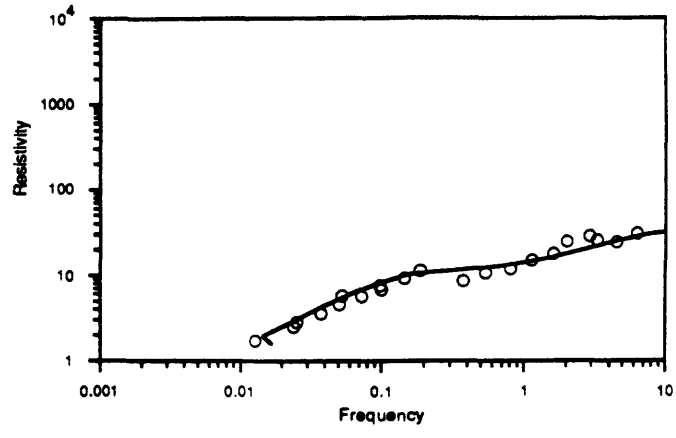

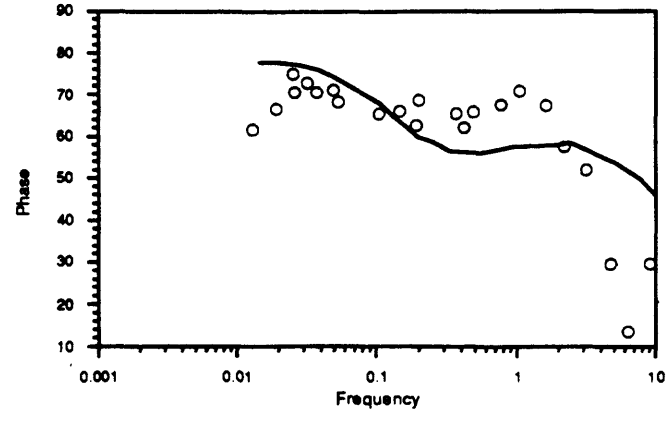

Station 31 - 1D Inversions

XY Polarization

km	
.1	5.9 Ω m
.5	20 Ω m
3	2.5 Ω m
	.3 Ω m

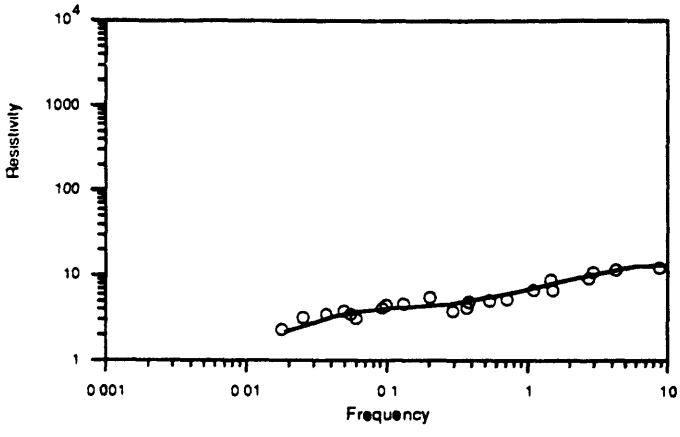

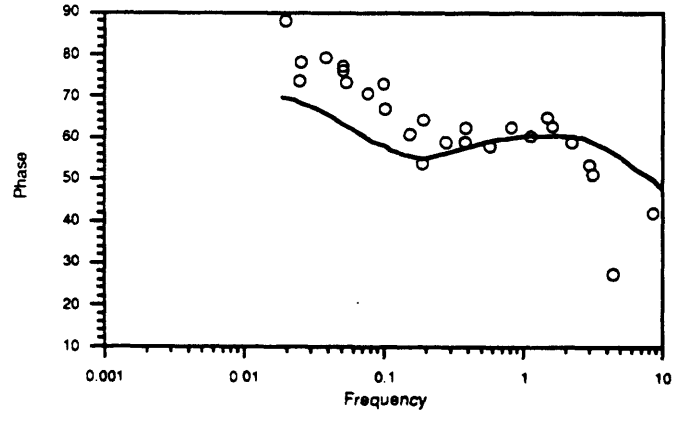

YX Polarization

km	
.08	5.5 Ω m
.4	20 Ω m
2.4	1.8 Ω m
	.1 Ω m

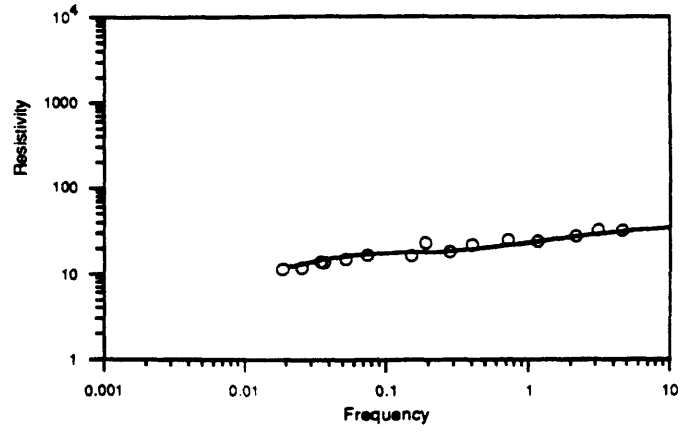

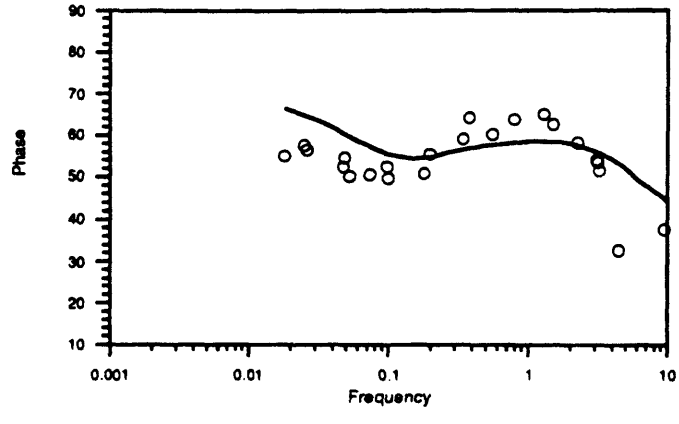

Station 32 - 1D Inversions

XY Poiarization

km	
1.1	110 Ω m
13	31000 Ω m
	12 Ω m

YX Poiarization

km	
.03	6.6 Ω m
24	8400 Ω m
28	730 Ω m
	70 Ω m

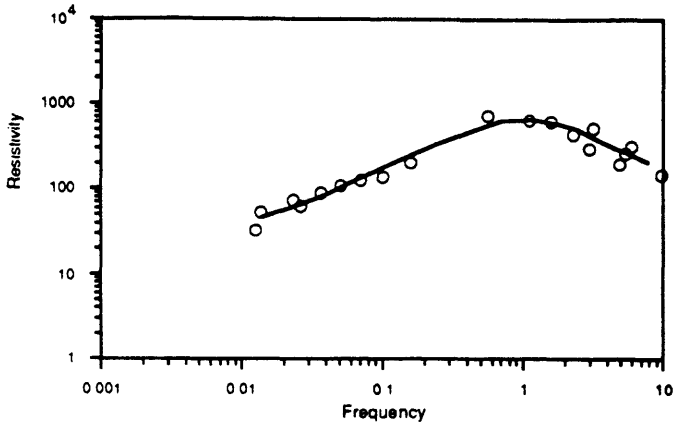

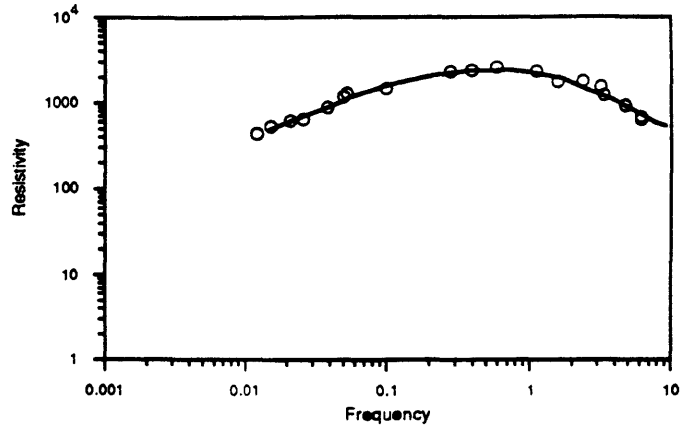

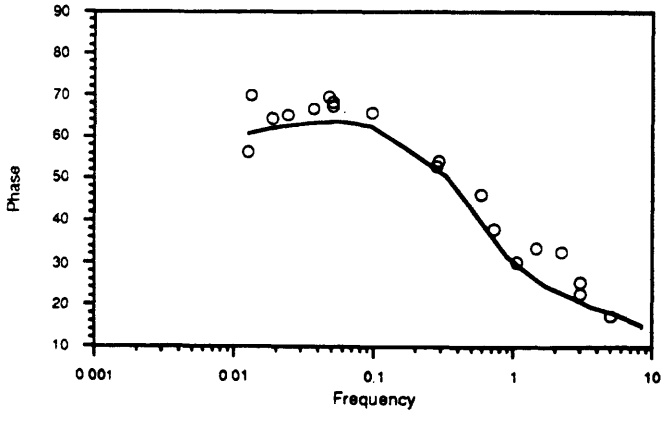

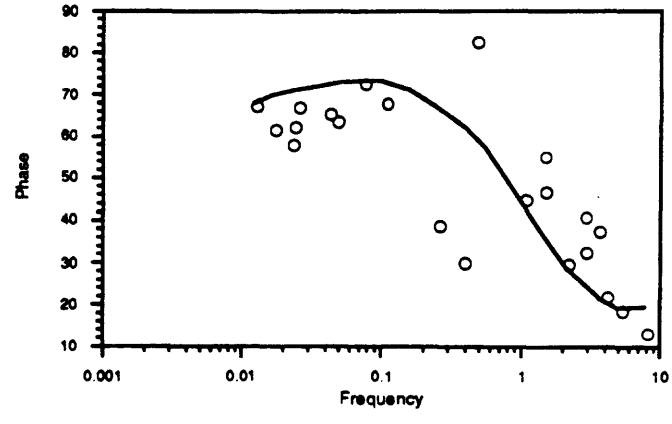

Station Argonaut 27 - 1D Inversions

XY Polarization

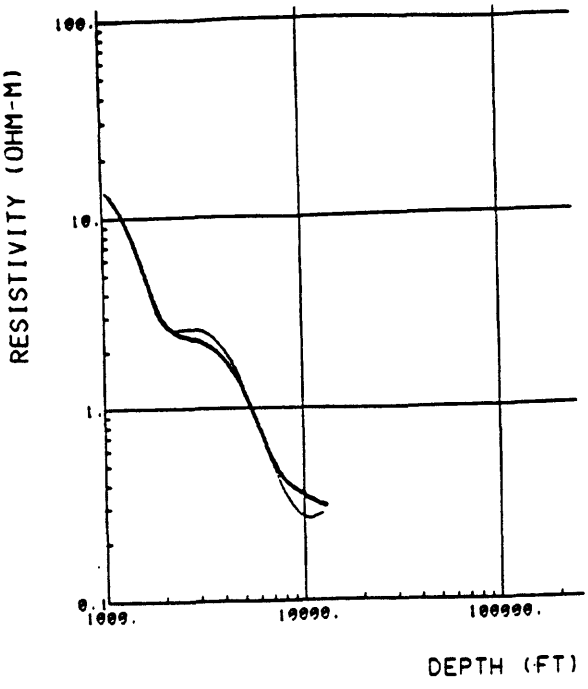

YX Polarization

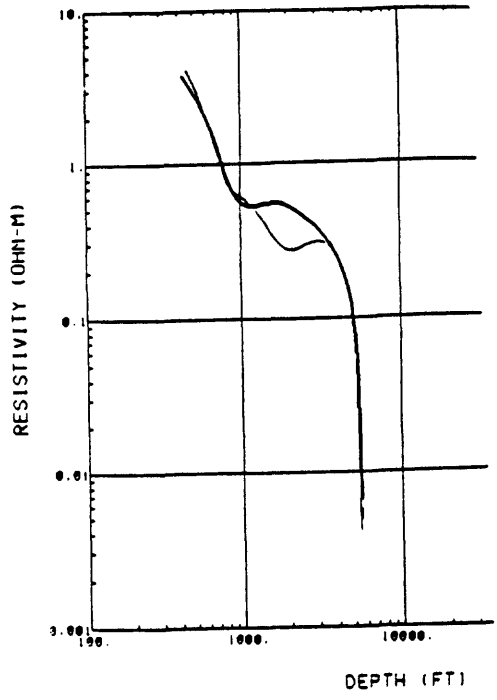

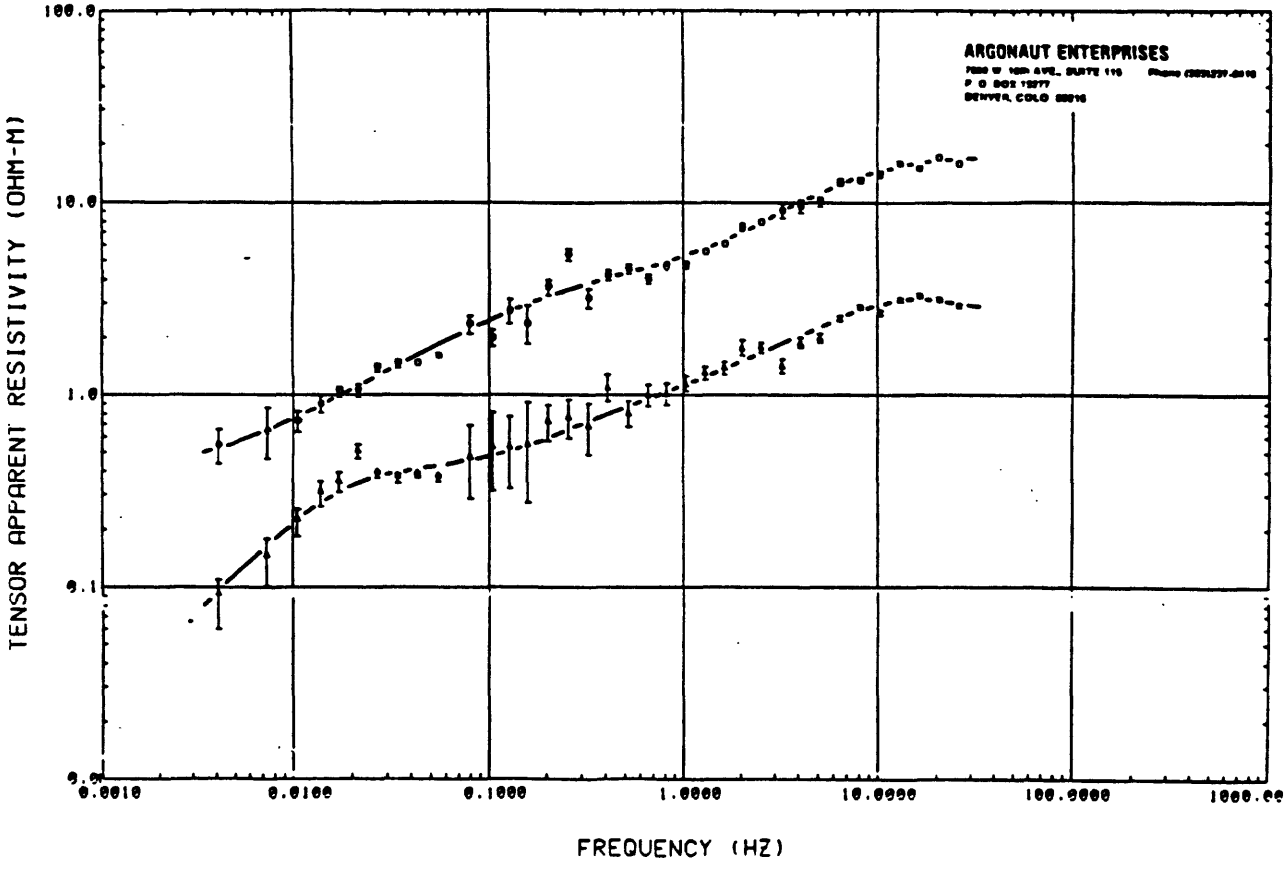

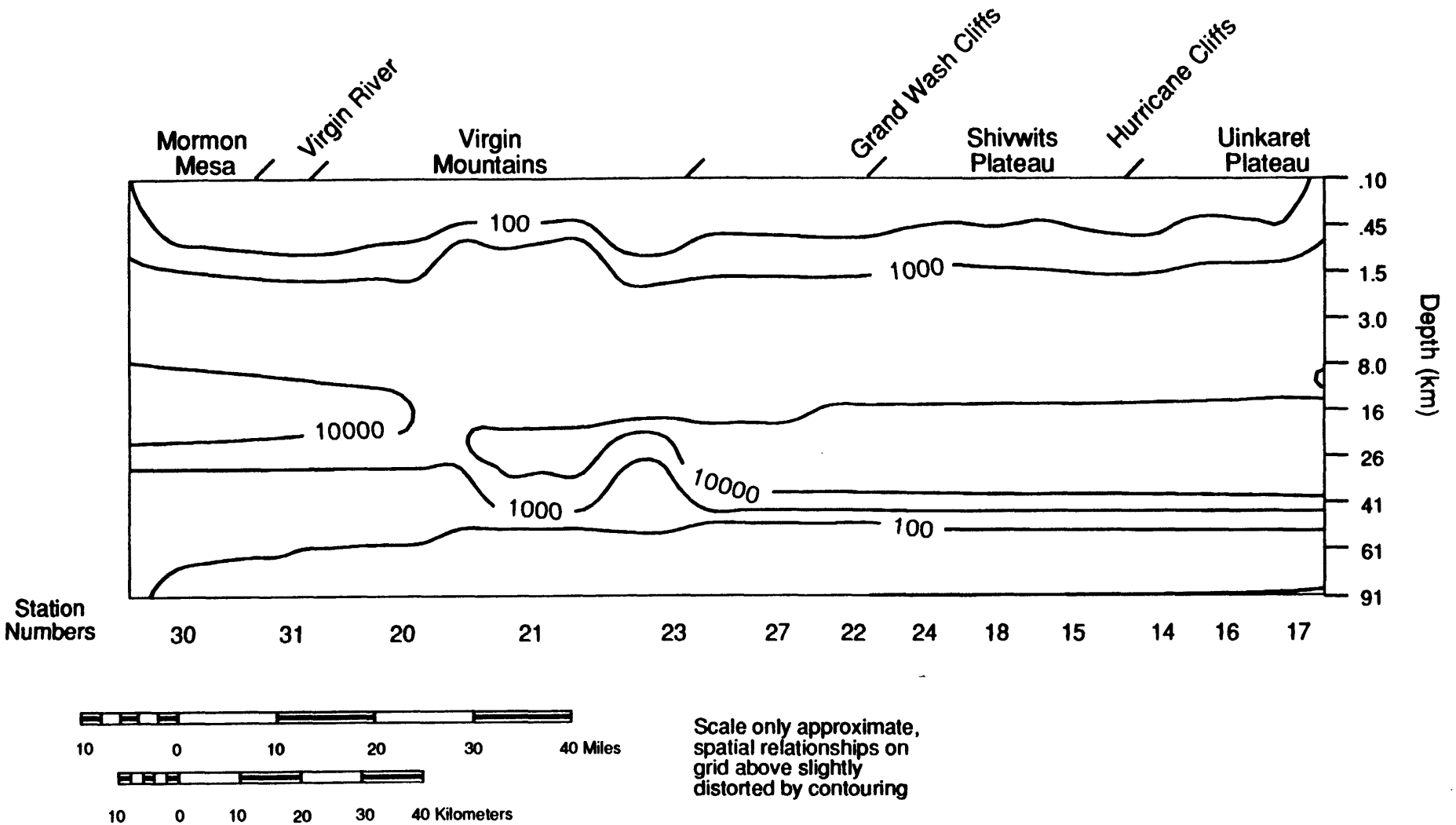

Fig. 5 -- 2D - Inversion results showing apparent resistivity. "Crustal" model. Data was modelled with a highly resistive middle layer. Inversions were based on fitting the TM mode whose axis was inferred from gravity data (Lysonski and others, 1981a, 1981b.).

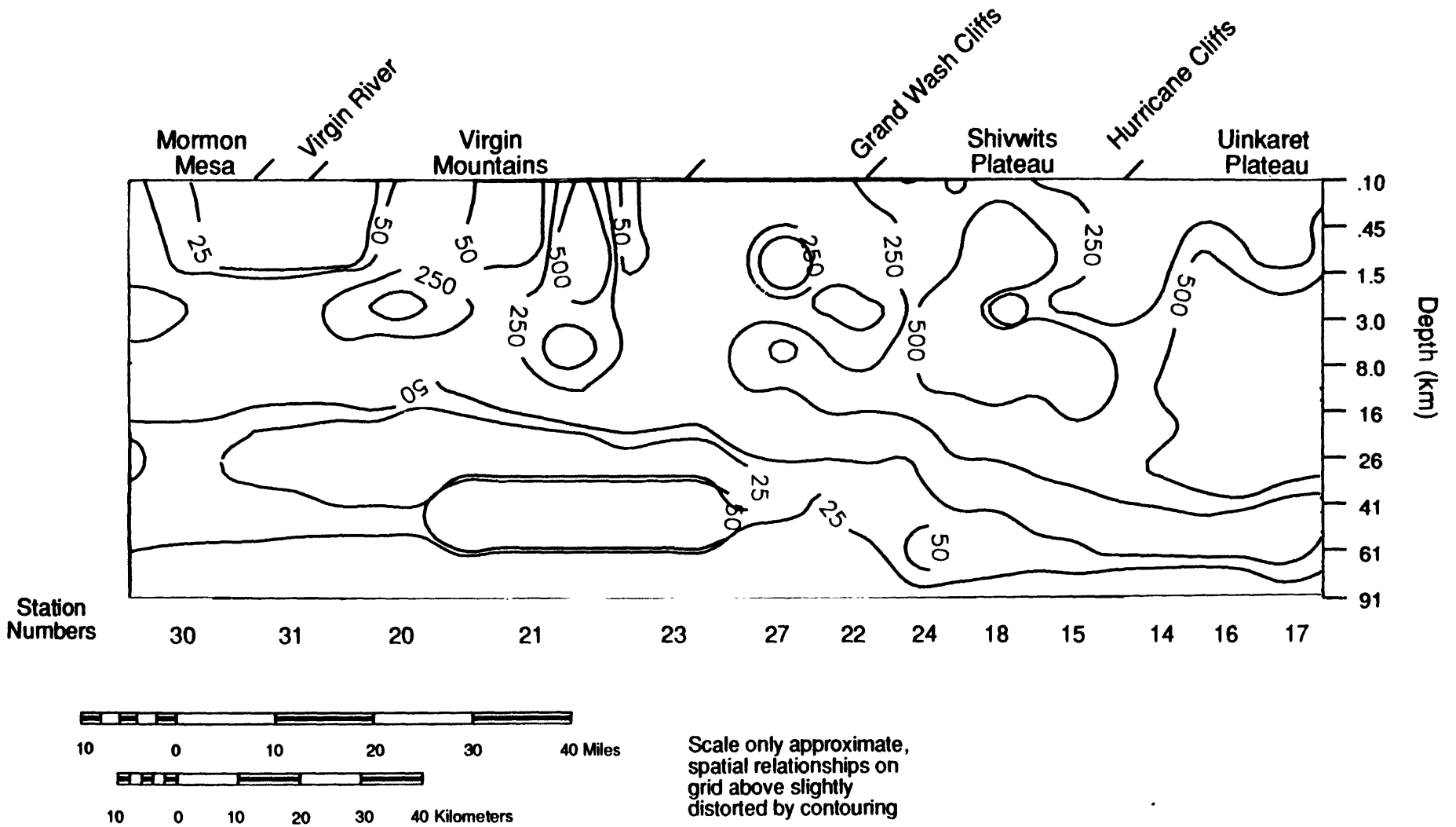

Fig. 6 -- 2D - Inversion results showing apparent resistivity. "No Crust" model. Data was modelled without a highly resistive middle layer. Inversions were based on fitting the TM mode whose axis was inferred from gravity data (Lysonski and others, 1981a, 1981b.).

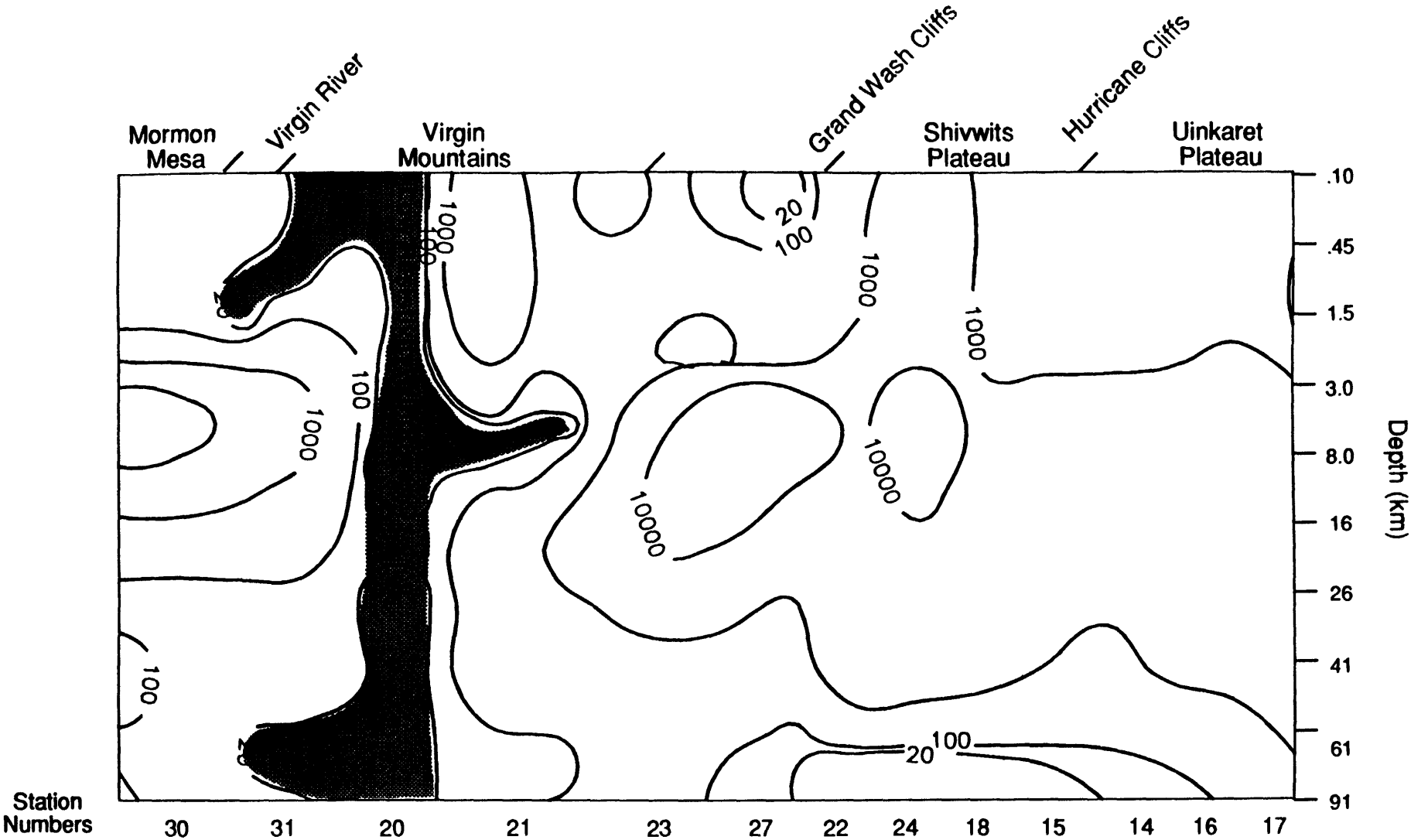

Fig. 7 -- 2D - Inversions results showing apparent resistivity. "Window" Model. Data was modelled without a highly resistive middle layer. This is the Best fit result with the most startling feature being the low resistivity "window" into the deeper surface. Inversions were based on fitting the TM mode whose axis was inferred from gravity data (Lysonski and others, 1981a, 1981b.)

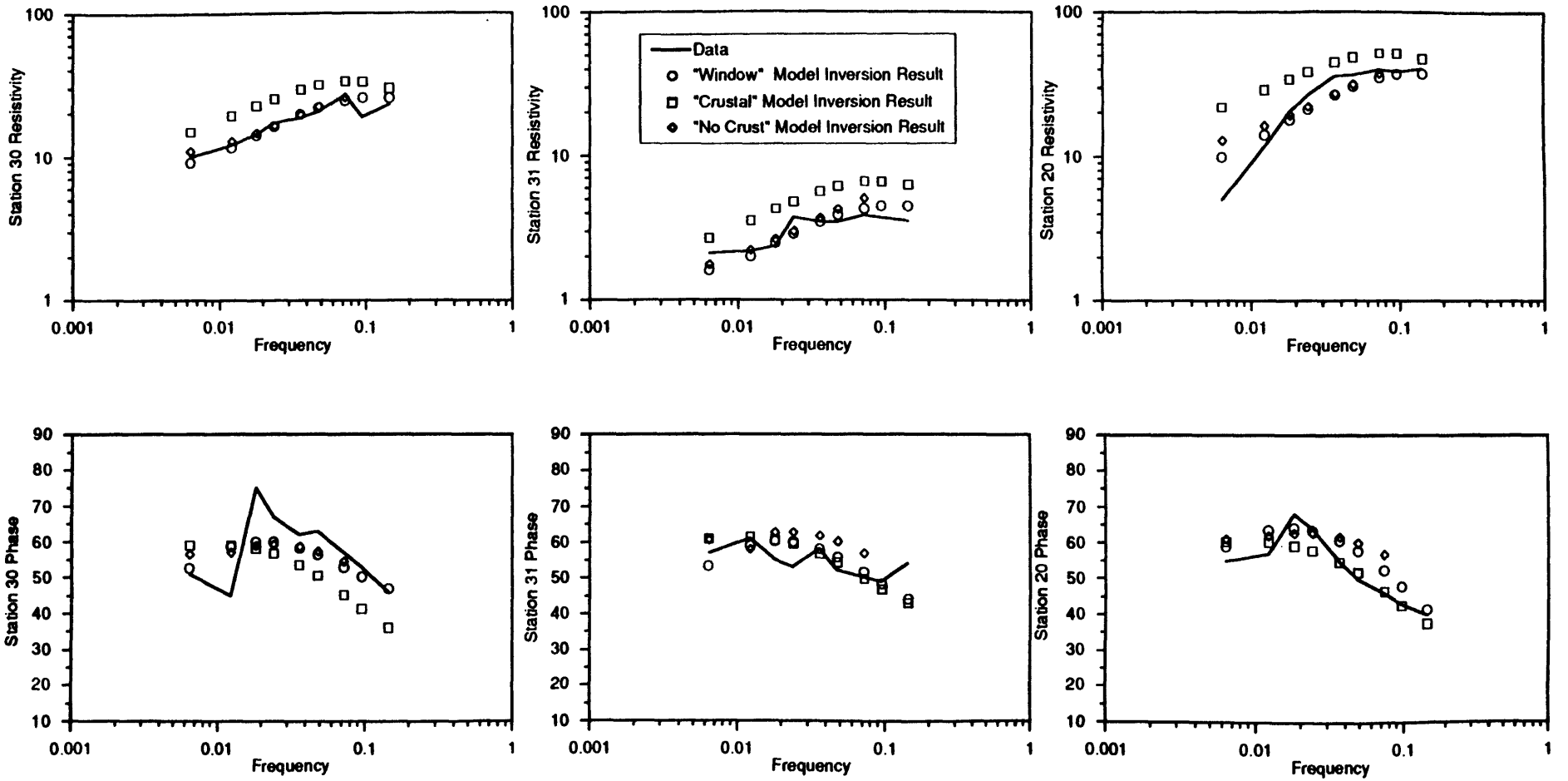

Fig. 8 -- Fit of modelled resistivity and phases versus data resistivity and phases for the two-dimensional inversions. Station 30 is the furthest west station and station 17 the furthest east. The fit to resistivity is much better than the fit to phase. The "crustal" model is an inferior fit and moreover the "window model" provides the best fit especially for phase.

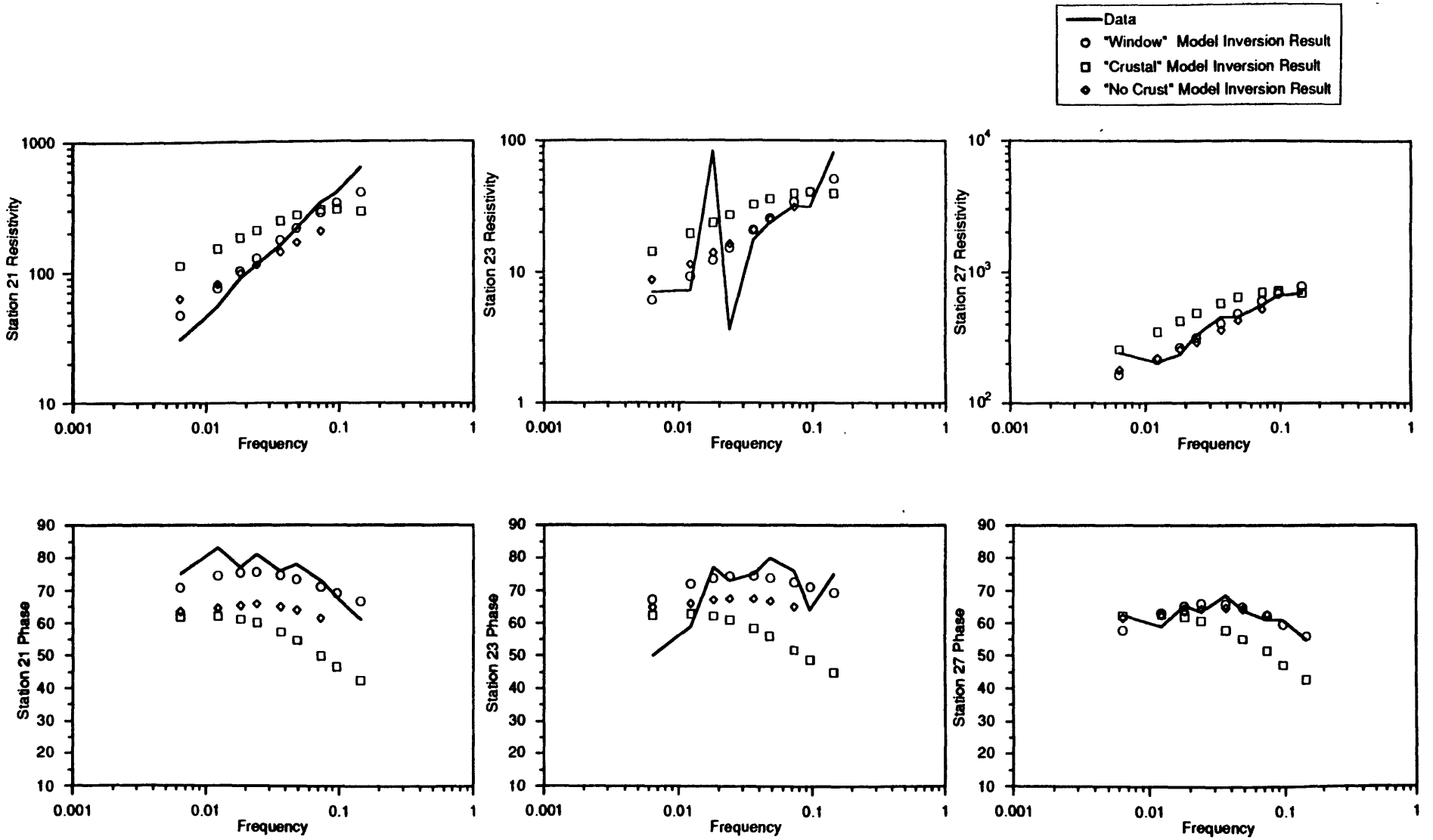
Data
"Window" Model Inversion Result
"Crustal" Model Inversion Result
"No Crust" Model Inversion Result
Station 21 Resistivity
Station 23 Resistivity
Station 27 Resistivity
Station 21 Phase
Station 23 Phase
Station 27 Phase
Frequency
0.001
0.01
0.1
1

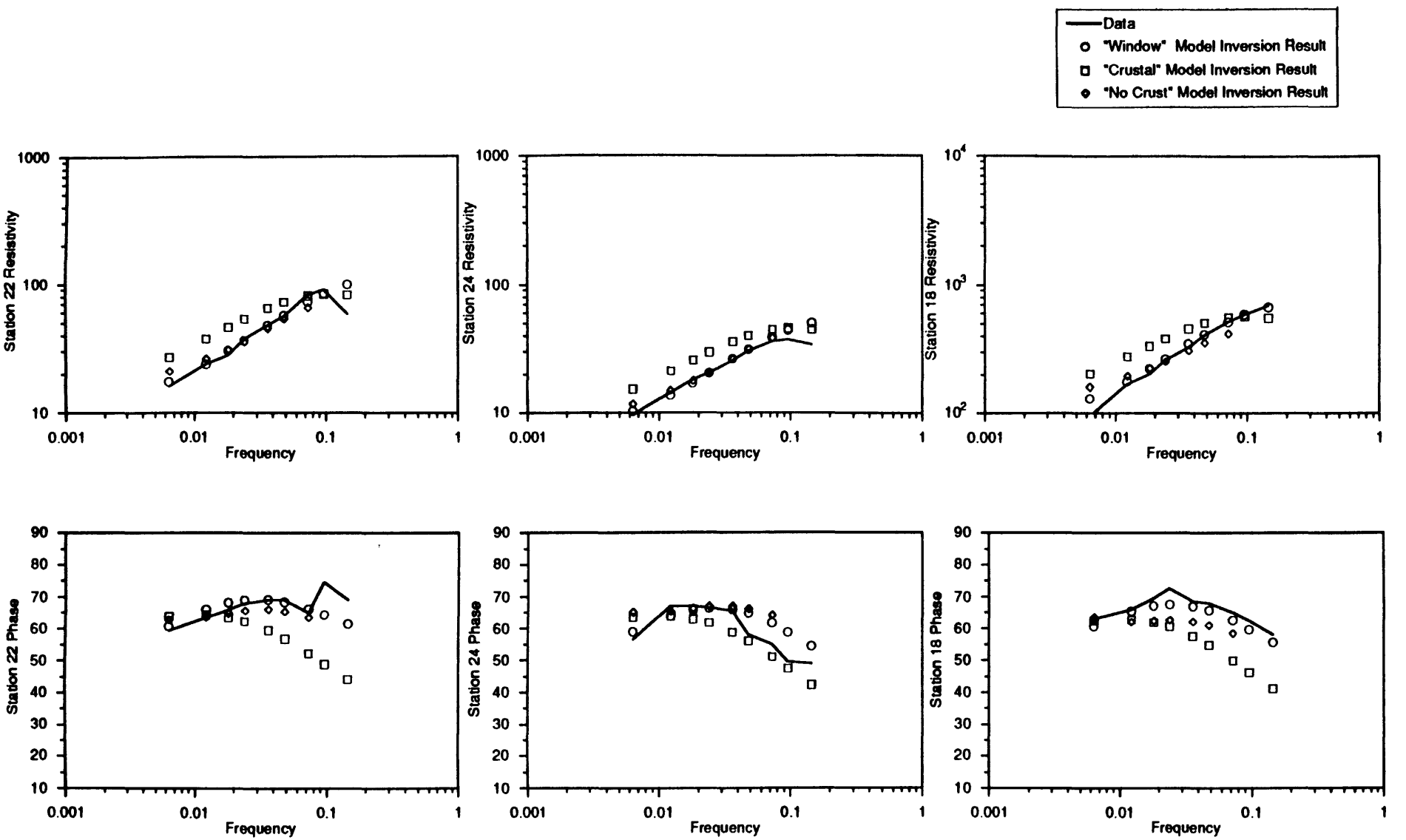
Data
"Window" Model Inversion Result
"Crustal" Model Inversion Result
"No Crust" Model Inversion Result
Station 22 Resistivity
Station 24 Resistivity
Station 18 Resistivity
Station 22 Phase
Station 24 Phase
Station 18 Phase
Frequency
0.001
0.01
0.1
1
10
100
1000
10^2
10^3
10^4
20
30
40
50
60
70
80
90

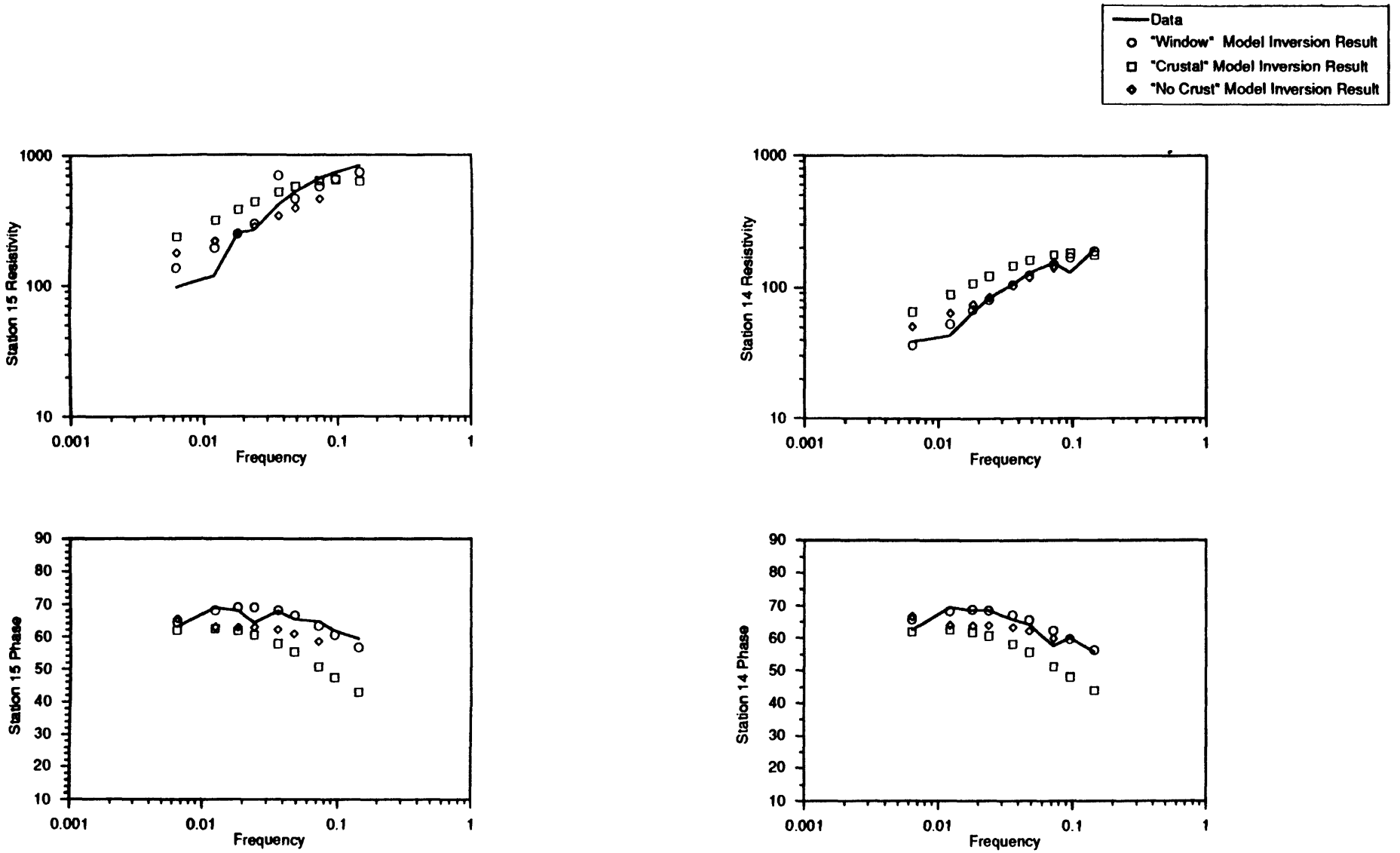
Data
"Window" Model Inversion Result
"Crustal" Model Inversion Result
"No Crust" Model Inversion Result
Station 15 Resistivity
Station 14 Resistivity
Station 15 Phase
Station 14 Phase
Frequency
1000
100
10
90
80
70
60
50
40
30
20
0.001
0.01
0.1
1

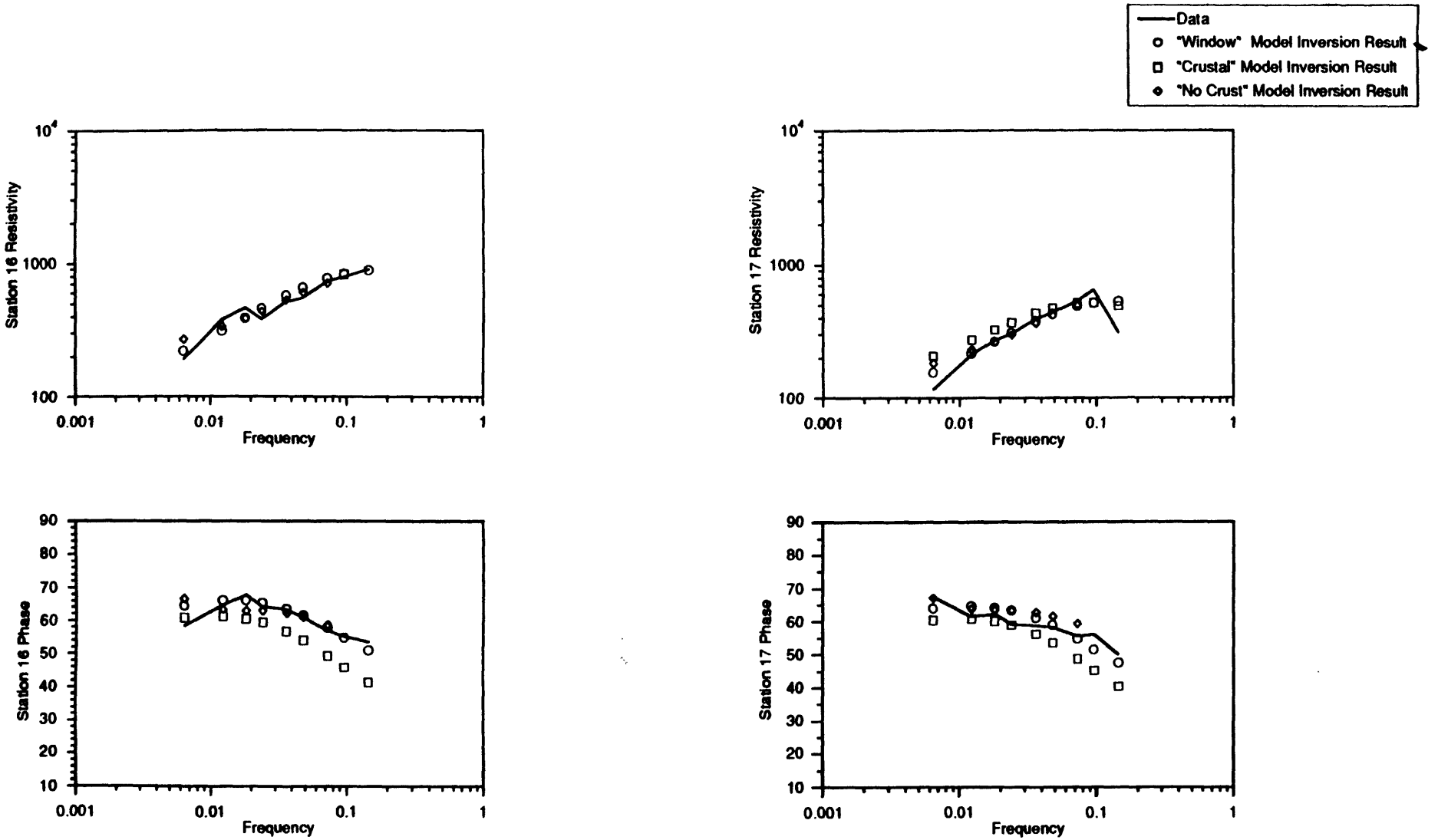
Data
"Window" Model Inversion Result
"Crustal" Model Inversion Result
"No Crust" Model Inversion Result
Station 16 Resistivity
Station 17 Resistivity
Station 16 Phase
Station 17 Phase
Frequency
0.001
0.01
0.1
1
100
1000
10^4
10
20
30
40
50
60
70
80
90